Insights from Megacryst-Included Zircon Dates on the Spatial Extent of Magma Mixing in the Tuolumne Intrusive Suite, California, USA

Elena Watts1, Julia Chen2, Sean P. Gaynor1,3, Valbone Memeti2, Blair Schoene1 Elena Watts1, Julia Chen2, Sean P. Gaynor1,3, Valbone Memeti2, Blair Schoene1 Corresponding author: Elena Watts (ewatts@princeton.edu)

Key Points:

- Megacryst-included zircon dates from megacrysts along a gradational contact between units can provide spatial constraints on magma mixing
- Magma mixing between two Tuolumne Intrusive Suite units likely occurred within a less than 2 km wide mixing front
- High precision U-Pb zircon ages from whole rock Cathedral Peak and porphyritic Half Dome samples are over 1.5 Ma apart

Abstract

The spatial extent of mixing between separately emplaced batches of magma is a key component in understanding the incremental assembly of plutons. Potassium feldspar megacrysts (>3 cm length) in granodioritic rocks are hypothesized to record magma mixing and transport over hundred kyr timescales. CA-ID-TIMS U-Pb dates from zircon inclusions within eleven new megacryst samples and their surrounding matrix from the Tuolumne Intrusive Suite are presented as a means of evaluating the extent of mixing across a less than two kilometer wide gradational contact. Megacrysts from within the gradational contact yielded included zircon dates consistent with mixing or transport from the older porphyritic Half Dome Granodiorite, but the zircon included in megacrysts from the younger Cathedral Peak Granodiorite show no evidence of interaction with the porphyritic Half Dome. These results, along with the trace element geochemistry of the zircon, suggest that the porphyritic Half Dome and Cathedral Peak magmas where we sampled were not comagmatic, which constrains the width of a mixing front to the kilometer scale gradational contact between these units. From within this gradational contact, we do find evidence of mixing consistent with prior studies. Differences between the core- and rim-included zircon date spectra also suggest that protracted growth is recorded in some K-feldspar megacrysts but may not be a requirement for forming them.

Plain Language Summary

Many silicic intrusions are thought to have been emplaced through multiple batches of magma into the mid- to upper crust. There is conflicting evidence as to whether or not these batches of magma mix and form larger, dynamic magma chambers at the emplacement depth. This study uses the dates of zircon included in large K-feldspar megacrysts to evaluate the spatial extent of mixing across a gradational contact between two units of an intrusive complex. Zircon dates from megacrysts sampled within the gradational contact are consistent with magma mixing having occurred as the megacrysts grew, but zircon in megacrysts from within the younger unit do not record mixing. This finding suggests that if magma mixing occurred between these units the mixing front was not wider than the gradational contact (< 2km).

1 Introduction

Based on abundant geologic and geochronologic evidence, the model of incremental assembly for pluton formation is largely accepted (e.g. Coleman et al., 2004; Farina et al., 2010; Gaynor et al., 2019; Matzel et al., 2006; Memeti et al., 2010 Schoene et al., 2012), but there is lingering uncertainty about the degree to which separate pulses of magma mix or mingle after emplacement. Understanding the extent of magma mixing at the emplacement level for upper crustal intrusions is critical for developing accurate models of volcanism and ore deposit formation (e.g. Gelman et al., 2013; Wilkinson, 2013). If magma-mush conditions are sustained between pulses in the upper crust, large and dynamically mixed magma chambers could form (Matzel et al., 2006; Memeti et al., 2022; Paterson et al., 2016; Žák & Paterson, 2005), yielding rocks which are hybrids of distinct magmas (Oppenheim et al., 2021). Alternatively, if each injection of magma is largely solidified before intrusion of the next pulse, mixing would be spatially restricted and focused at contacts if present at all (e.g. Bartley et al., 2006; Glazner et al., 2004; Horsman et al., 2009; Michel et al., 2008). Understanding these processes in the upper crust requires knowledge about the volume of distinct pulses and the timescales of their crystallization combined with field and laboratory evidence for the extent of mixing.

Magmatic minerals record the geochemical and geochronological history of liquid solidification. As a result, researchers are increasingly relying on mineral-scale geochemical data to evaluate models of magma transport, emplacement, crystallization and mixing (e.g. Ackerson et al., 2018; Barnes et al., 2016, 2019; Farina et al., 2014; Lackey et al., 2005; Oppenheim et al., 2021). A number of granitoid plutons around the world host potassium (K) feldspar megacrysts, which can exceed 5 cm in length, and commonly host abundant mineral inclusions, including zircon. U-Pb geochronology of these zircon inclusions has been used to estimate the maximum growth durations for the megacrysts and to assess the interconnectivity of temporally distinct magma injections (Barboni & Schoene, 2014; Chambers et al., 2020). Chambers et al. (2020) used this approach on a single megacryst from the Tuolumne Intrusive Suite (TIS) and argued the megacryst rims grew over as much as 0.5 Myr. They concluded that the core of the megacryst grew in an older batch of magma and the rim grew in a second, younger batch, suggesting the recycling of phenocrystic K-feldspars across potentially multiple kilometers. In this study, we build on these results by dating and measuring the trace element concentrations of zircons included in eleven new megacrysts and seven related whole rock samples collected across three units in the TIS: the porphyritic Half Dome Granodiorite (pHD), the younger Cathedral Peak Granodiorite to granite (CP), and the gradational transition zone between them (TZ), the latter being where the sample of Chambers et al. (2020) was derived. By leveraging the spatial coverage of our dataset, we estimate the extent of emplacement-level magma mixing between the pHD and CP during K-feldspar megacryst growth and inclusion of zircons. In our traverses we find this to be the width of the TZ, approximately one km. We use these data to compare and contrast to previous studies that have inferred larger scale mixing across the TIS using other minerals and markers (e.g. Paterson et al., 2016) or no mixing at the emplacement level (Bartley et al., 2006) to understand more fully the emplacement and crystallization history of this archetypal intrusion.

2 Geologic Background

The TIS is a metaluminous, concentrically-zoned intrusive complex in the Sierra Nevada batholith in California, USA, and formed as part of the Mesozoic arc along the western margin of North America. It is composed of five main units: the granodiorite of Kuna Crest (KC), the equigranular Half Dome Granodiorite (eHD), the porphyritic Half Dome Granodiorite (pHD), the Cathedral Peak Granodiorite (CP), and the Johnson Granite Porphyry (JP), which become younger, isotopically more evolved, and more felsic towards the center of the complex (Bateman & Chappel, 1979; Bateman, 1992; Coleman et al., 2004; Kistler et al., 1986; Paterson et al., 2016; Memeti et al., 2010). These units were incrementally emplaced over ~10.5 Myr in the Late Cretaceous (Coleman et al., 2004; 2012; Memeti et al., 2010; 2022; Paterson et al., 2016), and contacts between them vary from sharp to gradational over several km (Bateman et al., 1983). Geobarometry of the TIS indicates it intruded at pressures of 100-300 MPa (Ague and Brimhall, 1988).

Two interior phases of the TIS, the pHD and CP, are separated by gradational to sharp contacts. The pHD is characterized by K-feldspar phenocrysts up to 4 cm in length and some megacrysts exceeding 5 cm. It also contains up to 1 cm euhedral biotite and titanite, and up to several cm long sub- to euhedral hornblende. The transition zone (TZ) between the pHD and CP near Lyell Canyon is gradational and up to 650 m wide (Oppenheim et al. 2021) and is denoted by large K-feldspar megacrysts up to 12 cm long, and subhedral biotite and hornblende. In the CP, anhedral biotite grains are significantly smaller (~1 mm diameter) and hornblende is rare. K-feldspar megacrysts become gradually smaller toward the interior of the CP, but can reach up to 6 cm in length at the margins. K-feldspar pheno- and megacrysts in CP, the TZ, and particularly in the pHD contain numerous mineral inclusions, such as zircon, apatite, titanite, quartz, biotite, hornblende, and plagioclase, many of them aligned with crystallographic axes (Moore & Sisson, 2008; Vernon, 1986).

Early geochronologic studies using Rb-Sr isochron ages determined that the TIS formed over millions of years and that initial Sr isotopic ratios were inconsistent with the compositional variability within the TIS having derived from post emplacement fractional crystallization (Kistler & Fleck, 1994). Coleman et al. (2004) used multi-grain, physically abraded U-Pb TIMS zircon ages to show that multiple distinct pulses of magma incrementally assembled the TIS over ~9 million years. Burgess and Miller (2008) added to the U-Pb zircon dataset with single-crystal analyses of zircons from the CP, which they used to argue the CP crystalized over ca. 1 Myr. Memeti et al. (2010) dated more single zircons from the outer lobes of the complex, and interpreted shorter thermal and magmatic histories for the lobes. Paterson et al. (2016) summarized all TIS ages and interpreted “age gaps” particularly along the pHD-CP boundary arguing for magmatic erosion and removal and/or overprinting of magmatic records along sharp and gradational contacts. Most recently, Chambers et al. (2020) dated zircons included in a single megacryst core and rim (leaving out the mantle of the crystal) from the TZ and observed the majority of the zircon age distribution from the rim was younger than that of the core, from which they estimated a rim growth duration of over 0.5 Myr. The dates from the core are similar to ages obtained from published bulk-rock pHD, whereas rim dates trend towards published CP dates (see compilation in Paterson et al., 2016). Chambers et al. (2020) use these data to argue that the core of this megacryst grew predominantly in a parental magma with a pHD composition, was then transported or mixed with CP magma, and finally grew its rim in the pHD-CP transition zone. These geochronologic studies have established that the TIS grew incrementally and crystalized over ~10.5 Myr. This study attempts to further understand the spatial and temporal scales of magma mixing across the TZ during pluton construction.

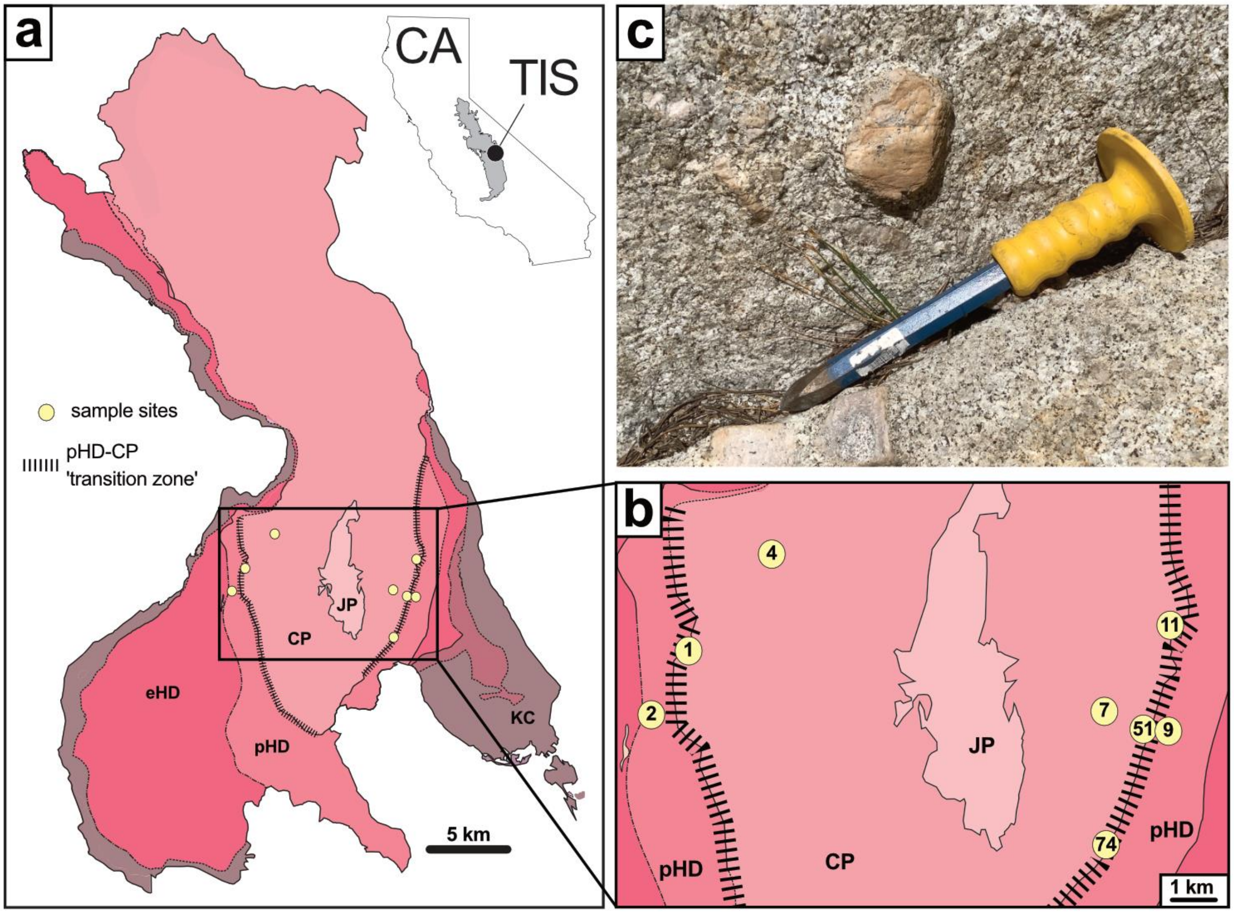

Figure 1 a) Simplified geologic map of the Tuolumne Intrusive Suite (TIS) adapted from Chambers et al. (2020). b) Inset of (a) showing sample site names. Sample site 74 refers to the LFO-74 sample location in Chambers et al. (2020). c) Photo of a TZ megacryst *in-situ* prior to sampling. Subunit abbreviations are as follows: granodiorite of Kuna Crest (KC), equigranular Half Dome Granodiorite (eHD), porphyritic Half Dome Granodiorite (pHD), Cathedral Peak Granodiorite (CP), and Johnson Granite Porphyry (JP)

3 Materials and Methods

Megacryst samples were collected as whole crystals from outcrop surfaces using a hammer and chisel where they had partially weathered out of the rock. They were then cleaned, mounted in epoxy resin, and bisected parallel to the (010) plane, i.e. perpendicular to the crystallographic *b* axis (Fig. A1-A2). At each sampling site, whole-rock matrix samples were also collected, and areas of high megacryst density were avoided for these samples. Megacrysts were cut into half sections and thin sections were made from the interior surfaces. For a subset of megacrysts, those from the west traverse, half of each crystal was sent to the University of Texas at Austin Computed Tomography (CT) lab for high-resolution CT scans (Fig. 2c) and the thin sections were taken to the Rutgers' Electron Microprobe Facility where backscatter electron (BSE) images were collected along transects with a JEOL JXA-8200 Superprobe. The CT scans were processed using Dragonfly software to render 3D density maps (Fig. A1). Using the zoning and abundance of mineral inclusions in the CT maps, core-rim boundaries were assigned and used to separate megacryst samples into separate core and rim sections with a trim saw. Care was taken in samples from the west traverse to remove all matrix material adhered to the crystal surface, which came at the expense of losing some of the outermost rim in some cases. In contrast, megacrysts from the east traverse were not imaged by CT, and were separated into core and rim sections based on mineral-inclusion density visible in hand-sample. To preserve as much rim material as possible small amounts of matrix were left on the east traverse megacrysts before crushing. Megacryst LFO-51 was processed using the same methods described in Chambers et al. (2020).

Zircon crystals were dated using chemical-abrasion isotope dilution thermal ionization mass spectrometry (CA-ID-TIMS) on the IsotopX Phoenix or the IsotopX Phoenix-ATONA at Princeton University as described in Appendix Text 1. For a number of samples, few (< 15) zircon crystals were separated, and therefor we performed neither CL-imaging nor in-situ geochemical analyses in order to preserve as much zircon material as possible for precise CA-ID-TIMS analyses. A correction for the initial ^{230}Th in the magma was made using a Th/U_{melt} composition of 2.85 ± 1.00 based on whole rock measurements of TIS samples in Gray et al. (2008). Dates from Chambers et al. (2020) are recalculated with this correction for direct comparison, though they do not change within uncertainty. Measurements of the ET100 synthetic zircon solution were collected alongside unknowns and have weighted average $^{206}Pb/^{238}U$ dates of 100.178 ± 0.008 (MSWD = 1.4, n = 15) and 100.167 ± 0.007 (MSWD = 1.1, n = 25) for the instruments with and without ATONA amplifiers (respectively) compared to the inter-laboratory calibrated date of 100.173 ± 0.007 (Schaltegger et al., 2021). Data were reported using the conventions of Condon et al. (2024).

Major and trace element concentrations of the dissolved zircons were measured on a Thermo Fisher iCAP ICP-MS in solution mode, using the column collects from the U-Pb separation (e.g., Schoene et al., 2010). All samples were dried down and brought back up in 1 ppb indium solutions to monitor sensitivity during mass spectrometry. A gravimetric matrix-matched external calibration solution was prepared to have the measured elements present in relative abundances similar to natural zircons. To monitor reproducibility, a solution with known Zr and Hf concentrations was measured repeatedly during analyses. The concentrations of elements in the acid washes can then be converted to concentrations by assuming that the combined zirconium and hafnium concentrations are equal to the stoichiometric concentration of zirconium in zircon (Schoene et al., 2010). However, to minimize systematic uncertainties from variability in partition coefficients as a result of temperature change and from the normalization process, zircon trace element concentrations are presented and interpreted as ratios (Rubatto & Hermann, 2007; Schoene et al., 2010).

4 Results

4.1 Megacryst Textures, Inclusions, and Zoning

From both traverses, pHD megacrysts are smaller than those from the CP or TZ with longest axes measuring approximately 5 cm. Our CP and TZ megacrysts range from 6 to 9 cm. All of the CT scans of megacrysts from the west traverse show some degree of concentric oscillatory Ba zoning, although the thickness and number of zones is variable (Fig. A1). In some instances less zonation is visible in the core (e.g. TIC2-BSbag, TIC4-VM1), which may indicate that these samples were not bisected at the exact center of the crystal. Perthite lamellae are visible in all BSE images from the west traverse, but the lamellae are larger and more abundant in the CP and TZ megacrysts. All of the megacrysts have visible mineral inclusions in CT and in hand sample (Fig A1-A2). In CT scans we interpret brighter inclusions as phases which are likely denser than the surrounding megacryst, such as hornblende or biotite, and darker inclusions as less dense phases such as plagioclase. These inclusions are generally smaller in the CP megacrysts than in pHD or TZ megacrysts (Fig. A1), and we observe this in the megacryst thin sections as well. Although zircon is a high density mineral and therefore should appear brighter than the surrounding K-feldspar in CT scans,he resolution of our scans is not sufficient to conclusively identify zircon grains, which are typically under 200 µm long in the TIS.

4.2 U-Pb Zircon Dates

We present 213 new zircon dates from megacryst cores, rims, and surrounding matrix in the TIS. We use ^{203}Th-corrected $^{206}Pb/^{238}U$ zircon dates for all of our interpretations because this chronometer provides the most precise and accurate estimate for samples of this age range (Figure 2), and all uncertainties are 2σ. For each megacryst with core- and rim-included zircon dates we calculated Δt, the difference between the youngest core-included date and the youngest rim-included date, and its uncertainty (Fig. 3). Where Δt overlaps zero within uncertainty we consider it to be unresolvable from our results. We interpret twenty-one of the dates shown in Figure 3 to be ante- or xenocrystic, meaning some or all of the zircon crystallized prior to the magmatism that formed the pHD and CP.

Most samples from the west traverse have dispersed zircon age spectra, where the youngest and oldest non-xenocrystic dates do not overlap within uncertainty, but generally decrease in age from the pHD to the CP (Fig. 2a). Two megacrysts from the pHD were analyzed, and the zircon ages from each sample have different relationships between core and rim. Youngest zircon dates from the core and rim of TIC2-BSbag overlap within uncertainty, and although Δt for this sample is below zero we note that a negative Δt is effectually the same as zero since the megacryst rim cannot predate the core (Fig. 3). This is likely caused by sampling bias given the low number of zircons retrieved from these samples, discussed more generally below. Conversely, the other pHD megacryst has a Δt of 0.49 ± 0.10 Myr. The youngest zircon dates from both megacrysts overlap within uncertainty with the youngest date from their surrounding matrix. One megacryst from the TZ was analyzed (TIC1-BS6) and yielded younger zircon dates from the rim than the core, with a Δt of 0.32 ± 0.18 Myr. The youngest rim date overlaps the youngest matrix date within uncertainty from this sampling site. Two megacrysts from the CP were analyzed along the west traverse, TIC4-VM1 and TIC4-EW17. The dates from the CP span ~ 1.27 Myr, with the exception of one xenocrystic age that matches the age range observed in the Kuna Crest. The range observed in the TZ is ~1.8 Myr and in the pHD is ~1.6 Myr. The youngest dates from the core and rim of TIC4-EW17 are indistinguishable within uncertainty, but TIC4-VM1 has a Δt of 0.46 ± 0.20 Myr. Similar to the TZ megacryst from the western traverse, the youngest matrix date is indistinguishable from the youngest rim dates from both megacrysts.

From the east traverse, one pHD megacryst was analyzed (Fig. 2b). This megacryst (TIC9-BS3) was too small to be separated into core and rim segments and was instead processed in its entirety. The range of dates from this megacryst is the same within uncertainty as the dates from its associated matrix sample but is offset towards older dates by approximately 300 kyr. Both megacrysts from TZ sample site TIC11 (TIC11-BS1 and TIC11-VM2) have unresolvable Δt's. However, the matrix age spectra from this sample site includes individual dates younger than those hosted by either megacryst by at least 0.5 Myr. The megacryst LFO-51 has a Δt of 0.44 ± 0.07 Myr, and the youngest matrix date from this site is younger than the youngest rim-included date. The CP age spectra from the east traverse are significantly less protracted, and nearly all the dates are within the same roughly 0.5 Myr time span, excluding three anomalously old dates that match with ages nominally found in the Half Dome unit. From this sample site we analyzed two megacrysts, one of which did not yield any zircons from the core (TIC7-VM4); for this sample only rim-included zircon dates are presented. We note that because small amounts of matrix material may have been attached to the rims of east traverse megacrysts (excluding LFO-51), there is a possibility that some zircons included in the rim fractions are derived from that matrix material. To accommodate this we utilize statistical methods in our interpretation which draw on the entire autocrystic date spectra of each sample.

We estimate final solidification ages for the matrix samples by assuming that zircon stops crystallizing at the solidus and that our zircon data approximate that time. To calculate this time, we use the Bayesian model of Keller et al. (2018; Fig 2; Table A3) with a bootstrap prior. Because this model can be heavily influenced by xenocrystic dates (Keller et al., 2018; Gaynor et al., 2023), older dates that we identified as inherited were excluded from this calculation.

When comparing solidification ages in the western and eastern transects, the two pHD samples are 88.61 ± 0.12 Ma and 89.09 ± 0.12 Ma, respectively, which do not overlap within uncertainty. Nor do the ages from the two CP samples, which are 87.04 ± 0.13 Ma from the west traverse and 87.33 ± 0.06 Ma from the east. The differences between the pHD and CP solidification ages are 1.57 ± 0.18 Myr and 1.76 ± 0.13 Myr for the west and east traverse, respectively. Three TZ samples have similar solidification ages of 88.17 ± 0.07 Ma (LFO-74; Chambers et al., 2020), 88.12 ± 0.06 Ma (LFO-51), and 88.03 ± 0.06 Ma (TIC-1), but the fourth TZ sample, TIC-11, has a younger solidification age of 87.60 ± 0.11 Ma. This age is younger than the nearest pHD sample's solidification age and older than the nearest CP sample's, noting that TIC-11 is offset northward from the rest of the traverse by ~2.5 km.

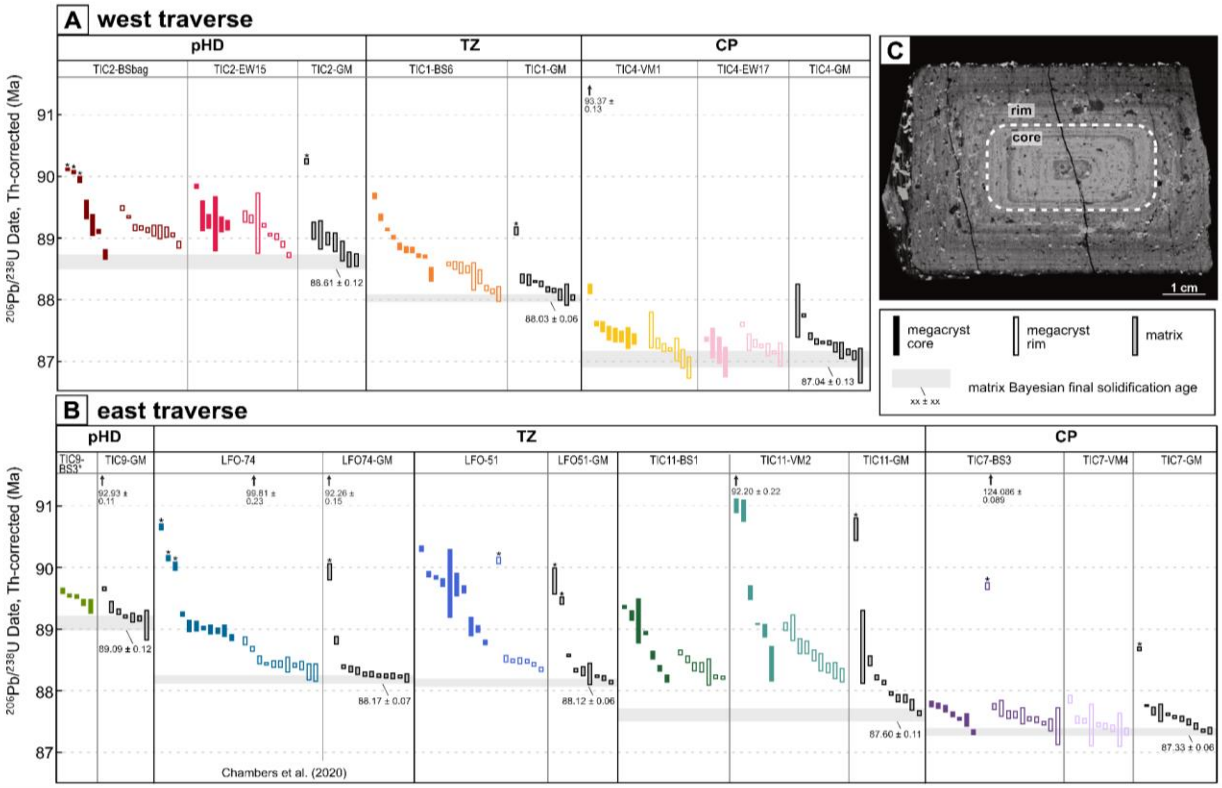

Figure 2 Rank order plots of $^{206}Pb/^{238}U$ zircon single crystal dates from the west (A) and east (B) traverses. Vertical bar heights are 2σ analytical uncertainties for individual analyses. Sample sites are separated by solid lines; megacrysts are differentiated by color and thin vertical lines; core-included zircon are shown with filled symbols and rim-included zircon are unfilled; matrix zircon are shown as gray symbols with black outlines for all sample sites. Upward arrows and * indicate inherited dates excluded from K-S testing and Bayesian modeling. Data from Chambers et al. (2020) are included. Gray bars indicate Bayesian-modeled final solidification ages for matrix samples after Keller et al. (2018), and are also presented at the 2σ level. (C) CT scan of sample TIC1-BS6. The dashed line shows where the core-rim boundary was assigned. Bright regions indicate areas of high density and dark regions are areas of low density. Concentric oscillatory zoning across the sample is interpreted as Ba zonation.

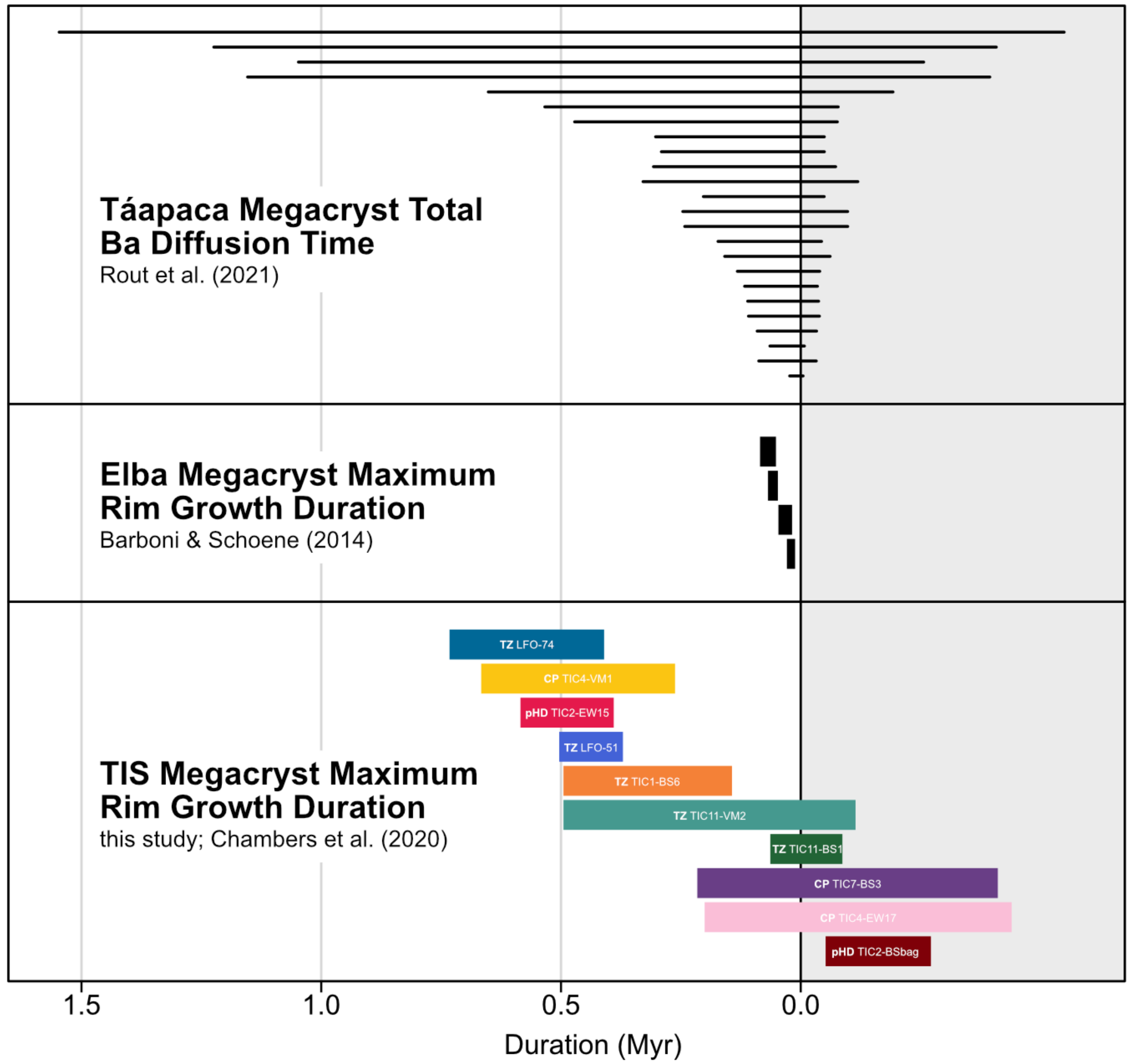

Figure 3 Estimates of whole or partial megacryst growth durations from this study, Chambers et al. (2020), Barboni & Schoene (2014), and Rout et al. (2021). Uncertainties are 2σ. Estimates from Tuolumne and Elba are calculated by comparing the youngest core-included zircon date to the youngest rim-included zircon date, and are predicated on the assumptions that the youngest matrix date approximately records when the solidus was reached and that no feldspar growth occurred after that point. See text for further discussion.

4.3 Zircon TIMS Trace Element Analyses

All trace element measurements are given in Table A2, but we have focused our interpretations here on three trace element ratios relevant to magmatic geochemical evolution. Dysprosium (Dy)-ytterbium (Yb) ratios in zircon may correspond to the growth of MREE compatible phases, such as apatite, titanite, and hornblende (Brophy et al., 2011). The average Dy/Yb of zircon from all sample types decreases from the pHD to the CP, but high Dy/Yb values are present in all three units (pHD, TZ, and CP), regardless of host magma. Within each subunit, Dy/Yb ratios do not appear to correlate to zircon dates (Fig. 4). Zirconium (Zr) -hafnium (Hf) ratios in zircon are sometimes used as a proxy for magmatic differentiation (Claiborne et al., 2006). Zircon Zr/Hf ratios show no strong correlation with zircon dates, within or across subunits. However, the lowest Zr/Hf ratios (<38 Zr/Hf) are from matrix zircon in all subunits. Thorium (Th) over uranium (U) ratios are calculated from TIMS measurements (Fig. 4). In the TZ and CP, Th/U ratios of matrix zircon span a lower range than megacryst core and rim zircon, however, Th/U ratios do not correlate with zircon dates throughout the data set. Overall, there appears to be trace element variability at the subunit and sample-type scales, but there are no direct correlations between zircon dates and trace element compositions. Matrix zircons, regardless of age, have populations with trace element ratios distinct from those in megacrysts.

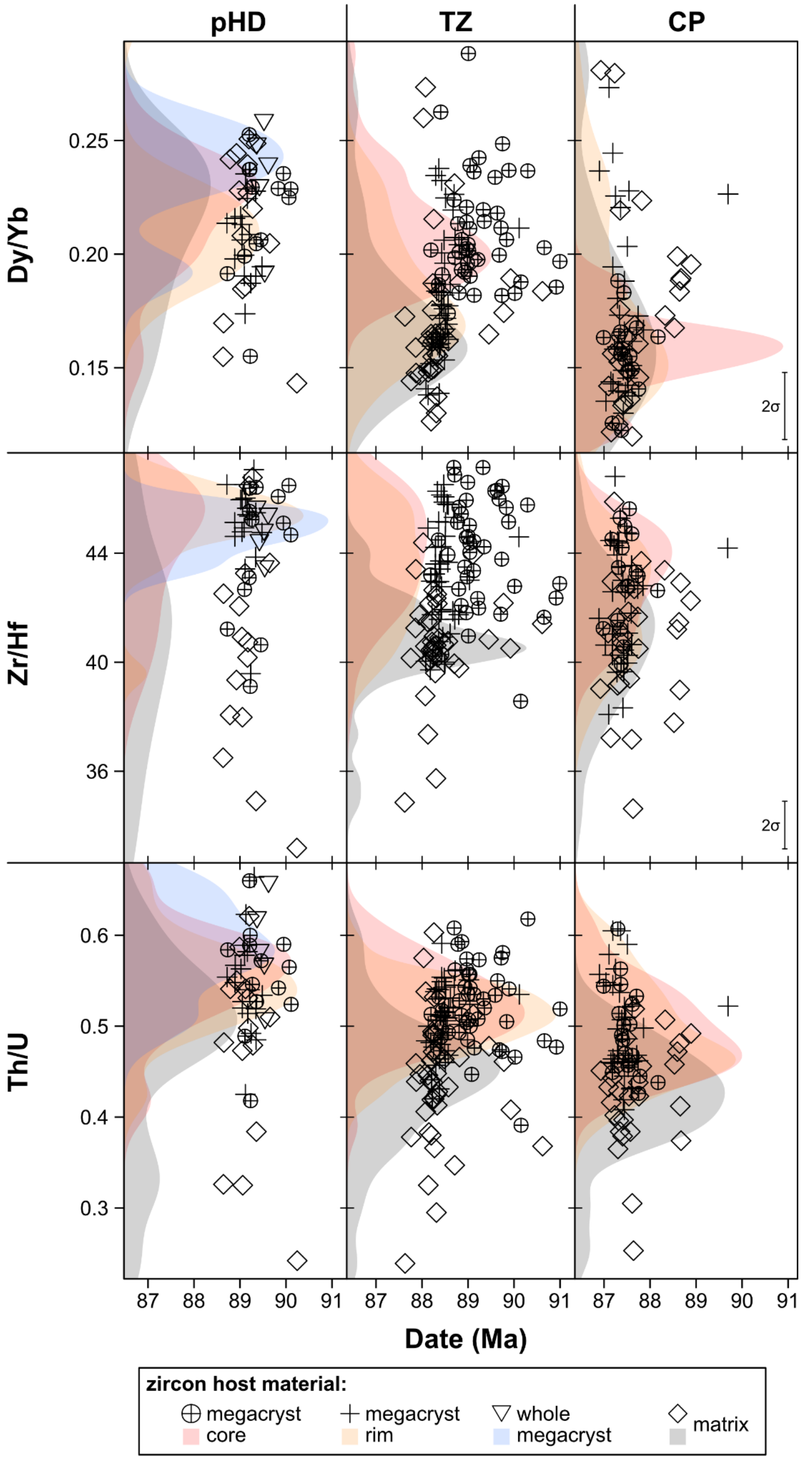

Figure 4

Zircon trace element compositions. Samples from both traverses are grouped by type, and data from Chambers et al. (2020) are included. Points show trace element ratios against date; semi-transparent curves are kernel density plots of the trace element ratios. Some extreme values are excluded from all plots; see Table A2 for full data reporting. There is significant overlap in the distributions of megacryst included zircon for all three trace element ratios, but matrix zircon have Th/U and Zr/Hf compositions that skew lower than megacrysts for all three subunits.

5 Discussion

5.1 The Temporal Record Within TIS K-feldspar Megacrysts and Surrounding Matrix

Improvements to precision in CA-ID-TIMS zircon geochronology over the last decade have yielded increasingly complex data sets, requiring more critical interpretations of plutonic dates (e.g. Eddy et al., 2022; Samperton et al., 2015). Incremental emplacement, inheritance, and extended trans-crustal growth histories can all contribute to protracted age spectra within igneous rocks (e.g. Tapster et al., 2016), and all can complicate interpretation of the timing and duration of intrusive emplacement, crystallization, or magma mixing. An assumption in the design of this study is that megacrysts randomly sampled zircon from the population present in the melt during K-feldspar crystallization. When comparing the core- and rim-included zircon dates from a megacryst and those from the matrix, we are ultimately trying to determine if there is a difference in the zircon populations these grains were drawn from. These differences, or lack thereof, can be interpreted to be the result of processes like magma mixing or protracted crystallization. To do this, we compare the full zircon date spectra, sans xeno- and antecrysts, by using the numbers calculated above for comparison (Δt, modeled crystallization ages) and also introduce a new approach using a modified Kolmogorov-Smirnov test.

5.1.1 Megacryst-Included Zircon Record

Differences between the youngest zircons from core and rim in megacrysts, quantified with Δt, may be interpreted in multiple ways. These include prolonged or sporadic megacryst growth within a single magma, such that the rims include zircons that crystallized after the core; mixing or erosion and transport of a megacryst core into a younger magma injection with subsequent growth of the rim including younger zircons; or a combination of these. For a given megacryst with a rim-included date spectra similar to the surrounding matrix dates, it is difficult to distinguish between an extended growth history in situ and mixing of an older megacryst core into a younger magma, as either could result in older zircon in the megacryst core. However, using the spatial context provided by analyzing multiple megacrysts across two traverses, we can better address the origins of Δt by comparing core and rim age spectra to possible sources of inherited cores (e.g., the pHD).

Observed core-rim Δt from the TIS megacrysts range from 0.5-0.3 Myr in half the megacrysts, (e.g. LFO-74; Chambers et al., 2020) and are unresolvable in other samples (e.g. TIC7-BS3). While the largest core-rim offset is observed in a TZ sample, at least one megacryst analyzed from each subunit of the west traverse has resolvable temporal differences between the youngest core and rim dates. The large core-rim offsets from most TZ samples may be the result of extended melt residency, magma mixing, or both as described above. Conversely, data from samples with unresolvable Δt, like TIC7-BS3, demonstrate that the rims of megacrysts need not grow over hundreds of thousands of years, and can grow over timescales similar to the precision of our zircon dates (tens of kyr).

Across all sample sites, young megacryst-included zircon dates are typically older than or overlapping with matrix dates, and in some instances matrix age spectra span younger by as much as 0.5 Myr. Sample site TIC11 exhibits a 0.5 Myr difference between the youngest megacryst hosted zircon and the crystallization date for the matrix, and interestingly it yielded the only TZ megacrysts without core-rim offset, suggesting zircon crystallization was significantly more protracted than megacryst growth in these megacrysts. One process that could explain the megacryst-matrix difference is that the megacryst grew elsewhere and was transported into a younger host matrix. Alternatively, K-feldspar growth is just as protracted as zircon growth with the last 0.5 Myr difference represented by dendritic K-feldspar growth in a crystal-rich mush (Gordon & Wallis, 2024), not captured in our dated megacrysts.

We note that in some megacrysts, the youngest core date is not overlapping within uncertainty with other dates from that core (e.g. TIC7-BS3), and that this could indicate Pb-loss affected these grains. Excluding these grains would make Δt resolvable for two of the megacrysts for which the core dates are very dispersed (TIC11-BS1, and TIC11-VM2) and nearly resolvable for TIC2-BSbag and TIC7-BS3 such that Δt would become 0.056 ± 0.059 and 0.09 ± 0.34 Myr for them, respectively. While it is impossible to rule out the effects of Pb-loss entirely, we consider this possibility unlikely given all these grains were chemically abraded, are concordant (Table 1), and overlap with young matrix dates from the same sites demonstrating that they are plausibly sampled from the same population. For Pb-loss to have generated these younger dates offset from the rest of the population, Pb-loss would have to coincidentally result in zircons from the core or rim or megacrysts that are the same as the youngest matrix zircon, which is possible but seems unlikely. Nevertheless, we use the K-S test described below to evaluate differences in core-rim zircon populations in part because it utilizes the entire date spectra and is not particularly sensitive to differences in distribution tails (e.g., young outliers).

We use a statistical approach to evaluate whether or not zircon populations from core, rim and matrix could have been sampled from the same population in an attempt to bring an objective approach to evaluating our data. From this we can then ask questions about whether differences, or lack thereof, resulted from magmatic processes. Standard two-sample two-sided K-S tests evaluate the null hypothesis that the distributions of two samples are identical by comparing their cumulative density functions (CDF; Massey, 1951 and references therein). In this case, we use the zircon dates and their gaussian uncertainties from a sample to create the compared CDFs. A detailed discussion of this statistical approach and potential applications of it to other datasets is provided in Appendix Text 2. This modified K-S test is a useful tool for quantitatively identifying variability between samples that may not be readily apparent otherwise. We ran a total of 41 modified K-S tests on the geochronologic data from this study and Chambers et al. (2020; Table 1). A test that yields a p-value below 0.05 rejects the null hypothesis and indicates it is unlikely the two samples were drawn from the same population, which in this context implies two zircon populations were included into their host materials from either different magmas and/or at different times within our analytical uncertainties. Xenocrystic and antecrystic dates were excluded from K-S testing, as were samples with fewer than seven non-xeno- or antecrystic dates.

The seven tests which compare dates of zircon included in megacryst cores and rims largely support the interpretations made in previous sections. For example, comparison of the zircon sampled from the core and matrix of megacryst LFO-74 from Chambers et al. (2020)

yielded a p-value below 0.001, indicating that these distributions are dissimilar (Fig. 5a). On the other end of the spectrum, the core-matrix comparison of megacryst TIC7-BS3 yielded a p-value of 0.89, consistent with the core and rim drawing zircon from a similar magma (Fig. 5b). We expect that if there are changes in the magma's zircon population over the course of megacryst crystallization, this difference will be the most stark between megacryst cores and their surrounding matrix. Of the seven core-matrix comparisons, four yielded p-values below 0.05 and all seven are below 0.1 (Table 1). These tests suggest that in the pHD and the TZ megacryst cores sampled different zircon populations than the matrix, but the evidence for this is weaker in the CP samples.

Tests comparing megacryst rims and the surrounding matrix may be useful for evaluating the likelihood of megacryst transport into the host matrix, or if the matrix continued to crystallize zircon after the megacryst stopped or slowed its growth. Only two of these tests reject the null hypothesis at our significance threshold (α = 0.05), LFO-74 and TIC11-VM2. Chambers et al. (2020) interpreted their rim zircon date distribution to be roughly coeval with their matrix distribution, however considering the CDFs of these samples, it is clear that zircon continued to grow in the matrix. The same is true for TIC11-VM2. TIC11-BS1 and LFO-51, both from the east traverse TZ, have p-values below 0.1 but fail to reject the null hypothesis. A majority of matrix dates from these samples are younger than the rim-included dates, and a failure to reject the null hypothesis suggests this could be a product of undersampling. From the pHD and CP, none of the rim-groundmass comparisons reject the null hypothesis, consistent with the megacryst rims and matrix solidifying at similar times. All together, these results indicate that there was late-stage zircon growth not captured by the megacrysts in some parts of the TZ but not necessarily at the other sampling locations. Conversely, as noted by Gordon & Wallis (2024), K-feldspar megacryst growth may have continued, but instead was preserved as anhedral to dendritic crystals emanating from megacryst margins into a high-crystallinity magma after euhedral megacryst growth ceased. In this case, our field sampling approach would have missed the last stages of K-feldspar growth at low melt fractions, whereas matrix zircons may have continued to grow and been sampled for geochronology.

Core vs Rim				**Core vs Matrix**			
Megacryst	**D**	**p-value**	**n**	**Megacryst**	**D**	**p-value**	**n**
TIC2-EW15 (pHD)	0.41	0.46	14	TIC2-EW15 (pHD)	0.82	0.015	13
TIC1-BS6 (TZ)	0.83	< 0.001	19	TIC1-BS6 (TZ)	0.94	< 0.001	19
TIC4-VM1 (CP)	0.74	0.008	14	TIC4-VM1 (CP)	0.56	0.08	18
TIC11-BS1 (TZ)	0.51	0.21	14	TIC11-BS1 (TZ)	0.63	0.05	16
LFO-51 (TZ)	0.95	< 0.001	16	LFO-51 (TZ)	0.95	< 0.001	17
LFO-74 (TZ)	0.95	< 0.001	19	LFO-74 (TZ)	0.95	< 0.001	19
TIC7-BS3 (CP)	0.2	0.96	17	TIC7-BS3 (CP)	0.23	0.89	17
Rim vs Matrix							
Megacryst	**D**	**p-value**	**n**				

TIC2-BSbag (pHD)	0.59	0.07	17				
TIC2-EW15 (pHD)	0.39	0.42	15				
TIC1-BS6 (TZ)	0.51	0.12	18				
TIC4-VM1 (CP)	0.27	0.78	18				
TIC4-EW17 (CP)	0.19	0.98	18				
TIC11-BS1 (TZ)	0.61	0.06	16				
TIC11-VM2 (TZ)	0.7	0.006	18				
LFO-51 (TZ)	0.67	0.07	13				
LFO-74 (TZ)	0.61	0.02	22				
TIC7-BS3 (CP)	0.16	0.99	20				
TIC7-VM4 (CP)	0.34	0.54	19				
Matrix vs Matrix - Inter Subunit				**Matrix vs Matrix - Intra Subunit**			
Comparison	**D**	**p-value**	**n**	**Comparison**	**D**	**p-value**	**n**
TIC2 (pHD) v TIC1 (TZ)	0.91	< 0.001	16	LFO74 (TZ) v LFO54 (TZ)	0.18	0.98	18
TIC1 (TZ) v TIC4 (CP)	0.95	< 0.001	20	LFO74 (TZ) v TIC11 (TZ)	0.64	0.01	20
TIC9 (pHD) v TIC11 (TZ)	0.94	< 0.001	16	LFO51 (TZ) v TIC11(TZ)	0.56	0.10	16
TIC9 (pHD) v LFO51 (TZ)	0.93	< 0.001	14	TIC1 (TZ) v TIC11 (TZ)	0.49	0.13	18
TIC9 (pHD) v LFO74 (TZ)	0.95	< 0.001	18	TIC1 (TZ) v LFO51 (TZ)	0.23	0.78	16
TIC11 (TZ) v TIC7 (CP)	0.8	< 0.001	19	TIC1 (TZ) v LFO74 (TZ)	0.47	0.14	20
LFO51 (TZ) v TIC7 (CP)	0.94	< 0.001	17	TIC2 (pHD) v TIC9 (pHD)	0.74	0.008	14
LFO74 (TZ) v TIC7 (CP)	0.94	< 0.001	21	TIC4 (CP) v TIC7 (CP)	0.62	0.02	21

Table 1 Summary of results of K-S testing. D is the K-S test statistic, and n includes all uninherited dates from both samples. Data from Chambers et al. (2020) are used in comparisons involving LFO-74.

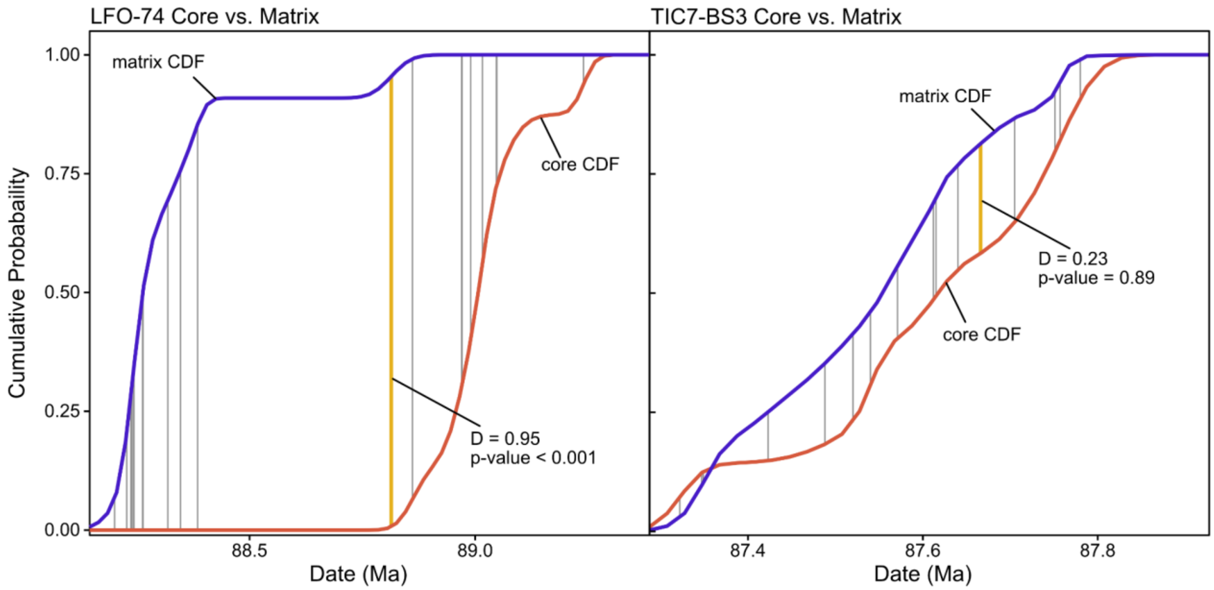

Figure 5 Visualization of modified K-S testing methods for the core vs groundmass comparisons of samples LFO-74 (left, Chambers et al. 2020) and TIC7-BS3 (right). Gray lines show where other dates from the samples fall on the x-axis and the distance between the CDFs at those points. The yellow lines show the dates where the difference between the CDFs is largest, which the test statistic, D, and p-value are calculated from. The left comparison is an example where the null hypothesis is rejected (p-value < 0.05), and we therefor interpret that the zircon crystals from the core of LFO-74 were likely sampled from a different population than the surrounding matrix. Conversely, the right comparison is an example where the null hypothesis is not rejected, and we do not rule out the possibility that zircon crystals from the core of TIC7-BS3 were sampled from the same zircon population as the surrounding matrix. A detailed description of modified K-S test methods, alongside additional applications of this tool, is available in Appendix Text 2.

5.1.2 Matrix Zircon Record

Modeled final matrix solidification ages are consistent with the spatial trends observed in previous studies of the TIS (Coleman et al., 2004; Paterson et al., 2016). We note that recent work has demonstrated that estimates of crystallization durations can be underestimated because zircon populations do not capture the time at which the solidus is reached based on thermal and geochemical modeling (Ratschbacher et al., 2018) and models of date-variability within individual zircon grains (e.g., Klein & Eddy, 2024; Curry et al., 2021; Tavazzani et al., 2023). However, we do not expect the size of these effects to change the broad temporal trends observed across the TIS.

The pHD, TZ, and CP subunits are all distinguished in part by megacryst size, mineral inclusion patterns, and abundance, and our data show that within all three subunits there is temporal variability. Three TZ sample sites have overlapping matrix final solidification ages, but TIC-11, which is closer to the inner TZ boundary with the CP, is up to 0.57 Myr younger (LFO74 vs TIC11; Chambers et al. 2020). Comparing matrix solidification ages from the pHD and CP between each traverse reveals variability as well (0.48 ± 0.17 and 0.29 ± 14 Myr, respectively), suggesting that exposures of texturally similar rocks mapped in the same subunit solidified at different times. This observation supports caution against using any of the solidification dates from our study for particular units to be representative for solidification of the same units elsewhere, which is supported by previous U-Pb geochronology documenting zircon age heterogeneity across individual map units (Coleman et al., 2004; Memeti et al., 2010).

In addition to K-S tests comparing megacryst-included dates, we also ran two series of tests comparing matrix date spectra to each other. The first series compares matrix samples between different subunits, and as expected these all yielded p-values below 0.05, consistent with published geochronology showing that these subunits of the TIS are temporally distinct (Memeti et al., 2022; Paterson et al., 2016). The second series compares matrix data between sample sites from the same subunit, and several of these tests also yielded p-values below our significance level. Our two pHD sample sites (TIC-2 and TIC-9) when compared have a p-value of 0.02, and our two CP sample sites (TIC-4 and TIC-7) yield a p-value of 0.008. Within the TZ sample sites LFO-74 and TIC-11, which are both from the east traverse but are several km apart roughly parallel to the contact, have a p-value of 0.01 when compared. These tests are further evidence that texturally similar rocks solidified at different points in time (e.g., Coleman et al., 2004; Shea et al., 2016; Tappa et al., 2011).

5.2 Melt Geochemistry Recorded by Zircon

Zircon trace elements record the geochemistry of the melt the zircon grew from, and when combined with U-Pb data, they can be a proxy for how magma chemistry changed through time (e.g. Schoene et al., 2010; Eddy et al., 2022). These data can be used to assess if zircon hosted in the cores and rims of megacrysts, the surrounding matrix, and different units of the TIS could have crystallized from geochemically similar magmas. One model of geochemical evolution across the TIS attributes geochemical variability to source composition, magma mingling and mixing during ascent, and fractionation and magma mixing at subunit-scales (over many km) during incremental emplacement (e.g., Memeti et al., 2010; Paterson et al., 2016; Oppenheim et al., 2021). Alternatively, others have proposed that this geochemical variability is primarily a result of changes in magma genesis prior to emplacement alongside fractional crystallization at the emplacement level on scales of no more than about a km (e.g., Coleman et al., 2012; Gray et al., 2008). By investigating changes in melt geochemistry through zircon included in megacrysts, we can better differentiate mixing- or fractionation-driven changes in magma chemistry from changes in source geochemistry. Within individual megacrysts we see limited variability in zircon Dy/Yb, Zr/Hf, and Th/U ratios (Fig. A3-A6). Instead, we focus our interpretations on all samples from the same subunit and host-material and make more general observations from the combined data.

The decrease in average Dy/Yb ratios (Fig. 4) from the pHD to the CP suggests that zircon in each successive unit grew in magmas that crystallized increasingly more MREE compatible phases or magmas with different starting MREE concentrations. Several MREE compatible phases are present in these subunits, particularly titanite, apatite, and hornblende. In addition to textural characteristics, the CP is distinguished from the TZ and pHD by a decrease in hornblende abundance (Bateman & Chappell, 1979). Therefore, if the decrease in Dy/Yb in CP relative to older units is in fact a result of increased crystallization of these phases, titanite or apatite would have to account for much of the decrease. Alternatively this trend may reflect changes in magma chemistry at the source level (Coleman et al., 2012), or the retention of hornblende crystals lower in the crust. In either case, these results suggest that the megacrysts from the successive subunits grew from geochemically variable magmas. Overlap in the Dy/Yb in zircon populations across the sampling transects is also consistent with mixing of zircon within the TZ. For example, TZ megacryst core zircons and pHD zircons have peaks in the KDEs at higher Dy/Yb ratios versus TZ rims and matrix, which in turn are trending towards Dy/Yb and ages in CP zircons. This is consistent with inmixing of at least two endmember magmas across the TZ as a function of time. Whether or not this trend is the result of mixing portions of zircon that crystallized in two end-member magmas or whether they record a gradual shift in magma chemistry (or some combination of the two) could be further constrained by in situ geochemical measurements of the zircons.

Zircon Zr/Hf ratios can be used as a proxy for magma fractionation, as zircon progressively crystallizes and preferentially extracts Zr from the melt over Hf (e.g., Claiborne et al., 2006). Zr/Hf ratios do not appear to systematically vary between subunits, and matrix zircon ratios range from overlapping with megacryst-included zircon to Zr/Hf compositions below 36, lower than any megacryst-included zircon (Fig. 4). Chambers et al. (2020) observed a larger offset between the Zr/Hf ratios of their megacryst-included and matrix zircon, wherein matrix zircon were consistently more evolved. They interpreted this as evidence that the last stage of crystallization of the matrix zircon was from a more evolved and zircon-fractionated melt than the megacryst-included zircon. Although we observe much more overlap in the Zr/Hf of megacryst-included zircon and matrix zircon, the zircon with the lowest Zr/Hf are all from matrix samples. Thus, we do not conclude that all matrix zircon across the subunits grew from a more evolved melt than the megacryst hosted zircon, but the low Zr/Hf matrix samples do suggest some zircon crystallization from evolved melts that megacrysts did not incorporate. Evidently a higher proportion of matrix zircon grew from evolved melt in the locale studied in Chambers et al. (2020) compared to the new sample locations. Interestingly, these low Zr/Hf zircon are not consistently younger than other zircon from the same subunit, indicating that these evolved melts may have existed at multiple times. Alternatively, these data could be explained by matrix zircons having young, low Zr/Hf, low U rims (so as to not impact the age) - a hypothesis that can be tested in future work.

Zircon Th/U is also used as a proxy for magma fractionation and is particularly sensitive to titanite and apatite crystallization (Schaltegger et al., 2009). Zr/Hf and Th/U are positively correlated in our dataset, despite U being four times more compatible than Th in zircon (Fig. A6; Mahood and Hildreth, 1983), and the low Zr/Hf matrix zircon typically have low Th/U ratios as well. This suggests there was sufficient titanite or apatite crystallization concurrent with zircon crystallization to deplete the Th/U composition of the melt. The lowest Th/U zircon are all from matrix samples, which indicates some matrix zircon (and titanite) grew from evolved melts not well recorded by megacrysts at potentially multiple points in time. One possible explanation for these low Zr/Hf and low Th/U matrix zircon is that the euhedral megacrysts did not capture those zircons grown during final crystallization in highly evolved melts. The K-feldspar may have instead continued to crystallize in anhedral, interstitial grains (see also Gordon & Wallis, 2024). Alternatively, the majority of megacryst growth took place during ascent, or the megacrysts grew in an ancestral magma that was overprinted by late evolved, percolating melts. This would be consistent with some degree of melt extraction over the course of fractionation as proposed by studies of feldspar and hornblende geochemistry (Oppenheim et al., 2021; Barnes et al., 2019). However, if this is correct, megacryst zircons do not record source signatures but reflect magma processes during ascent and at emplacement levels.

5.3 Megacryst Growth Histories

Previous geochronologic studies on K-feldspar megacrysts in magmatic systems have estimated the duration of megacryst growth. Barboni & Schoene (2014) concluded that the rims of megacrysts from the Elba intrusive suite grew over ~30 kyr. This is significantly shorter than the 500 kyr megacryst rim growth duration calculated by Chambers et al. (2020) on a TIS sample, but it is consistent with Elba having a short-lived melt-residence in the shallow upper crust after emplacement (Barboni et al., 2015; Farina et al., 2010). Rout et al. (2021, 2024) used Ba diffusion chronometry to estimate growth durations between 9 and 490 kyr for sanidine megacrysts from Taapaca Volcano. They interpret much of this growth to occur in small batches at shallow depths in the upper crust, prolonged by repeated temperature cycling from recharge events.

There are important considerations that go into calculating these durations from megacryst-included zircon dates. At the most basic level, the included zircon dates represent the timing of zircon crystallization, not their host feldspar. Although the feldspar must crystallize after any zircon it includes, how long after is difficult to determine. Some megacrysts exhibit differences in mineral inclusion type and density between cores and rims, which are often apparent in the field. In our samples, while we attempted to use textural (mineral inclusion alignment) and geochemical (Ba-zonation) features to guide core-rim boundary assignments on the megacrysts, we ultimately do not have enough information to attribute any petrologic significance to these boundaries. It is possible that the megacrysts grew in such a way that there is only minor petrologic distinction between the core and rim, and it is also possible that we did not correctly identify a significant core-rim boundary. As such we treat the boundaries we cut along as arbitrary in our interpretation and only assume that the core must crystalize before the rim. By dividing the megacrysts arbitrarily into separate core and rim sections, we obtain two age maxima for every megacryst: the youngest core date is the maximum age of the end of core crystallization, and the youngest rim date is the maximum age of the end of rim crystallization. Since both of these values are maxima, we cannot accurately calculate the duration of time between them. One possible solution to this problem is to assume no megacryst growth occurred after crystallization of the youngest rim zircon's date. This assumption is predicated upon the youngest matrix zircon approximately recording when the solidus was reached and that no subsolidus megacryst growth occurred. There is evidence against the former (e.g., Gordon & Wallis, 2024), and if interstitial growth was present around our sampled megacrysts it was not captured by our sampling. Regardless, if the youngest rim date is similar to the youngest matrix date, it implies that the megacryst grew until the solidus was reached within the precision of the zircon dates, and a maximum growth duration can be calculated (Fig. 3). The fact that this is a maximum duration is important, and ultimately makes the calculation less useful for understanding how much magmatic history is recorded in a megacryst. If a K-S test indicates a megacryst's core and rim zircon samples were likely drawn from different populations, it can be concluded the duration is greater than zero, but it does not indicate how much greater. Consequently, assessing megacryst rim growth durations from included zircon comes with uncertainties that are difficult to quantify, particularly in cases where the rim-included and matrix zircon date distributions are significantly different (e.g. TIC-11). These cases may be indicative of transfer of the megacryst into a new host matrix, or continued growth of K-feldspar as an interstitial phase.

Despite these issues with calculating a rim growth duration, there is still information to be gained about megacryst growth histories from the dates of zircon within them. One model for megacryst formation is that they form in near-solidus high-crystallinity magmas as a result of dissolution-re-precipitation reactions driven by temperature cycling (Johnson & Glazner, 2010; Glazner & Johnson, 2013). While this is obviously not the case for megacrystic sanidine found in volcanic rocks (Taápaca Volcano, Rout et al., 2021) or hypabyssal intrusions (San Martino porhpyry, Farina et al., 2014), our approach can test this model in plutonic settings. If the majority of a megacryst grew near or below the solidus, and the core and rim zircon were sampled from effectively the same population, there should be an equal chance of finding a younger date in the core as in the rim. However, of the fourteen total megacrysts that have been analyzed using this workflow between this study, Chambers et al. (2020), and Barboni & Schoene (2014), there is no instance where the youngest core date is younger than the youngest rim date. For all fourteen megacrysts the youngest core date is either equivalent within uncertainty to or older than the youngest rim date (Fig. 2; Chambers et al., 2020; Barboni & Schoene, 2014). The consistency of this pattern is evidence that megacryst growth is likely not a rapid near-solidus process, and it supports our interpretation that the zircon population in the melt changed over the course of megacryst growth in some instances (e.g. TIC1-BS6). There are other instances where our zircon dates conversely demonstrate that prolonged melt-residence is not necessarily required for megacryst growth, and that megacrysts grew faster than our method can resolve (e.g., TIC7-BS3). Several lines of evidence, such as Zr-in-titanite temperatures (Moore & Sission, 2008), intra-megacryst isotopic variability (Cox et al., 1996; Farina et al., 2014; Gagnevin et al., 2005; Kistler et al., 1986), and the low Zr/Hf matrix zircon not incorporated into megacrysts, all suggest megacryst growth predominantly occurs in hypersolidus conditions. However, these findings do not necessarily place constraints on growth rate in those conditions. Ultimately, it is possible for multiple magmatic processes to contribute to the formation of not only megacryst populations within a pluton but even individual megacrysts themselves.

5.4 Magma Mixing in the TIS

Over the last several decades, models for the amount of magma mixing, mingling, magmatic and host rock assimilation, and fractional crystallization at the currently exposed emplacement level of the TIS have evolved. Evidence for magma mixing in the TIS at the meter to kilometer scale is abundant. Several studies established mixing in the TIS using different markers (listed from large to small spatial scales and high to low hypersolidus temperatures) through plagioclase compositional zoning patterns (Memeti et al., 2022; Oppenheim et al., 2021; Wallace and Bergantz, 2002), enclave distributions (Barnes et al., 2021; Paterson et al., 2016), ante- and xenocrystic zircon populations (Miller et al., 2007; Paterson et al., 2016), cognate inclusions (Paterson et al., 2016; Žák and Paterson, 2005, 2010), and hornblende and K-feldspar populations (Barnes et al., 2016; Chambers et al., 2020; Oppenheim et al., 2021). The spatial and temporal scales and locations of mixing of each different marker remain somewhat uncertain. Wallace and Bergantz (2002), Oppenheim et al. (2021), and Memeti et al. (2021) use plagioclase (a liquidus phase) to interpret mixing of at least two plagioclase populations in all TIS units, arguing the pHD represents a more complex hybrid magma between eHD and CP (Oppenheim et al., 2021). This is consistent with enclave and antecrystic zircon mixing in all units (Paterson et al. 2016), some, but potentially not all of which likely occurred during ascent (Barnes et al., 2021; Memeti et al., 2022). Coleman et al. (2012) identified compositional layering within the eHD that they argued was caused by pulses of eHD magma that underwent post-emplacement fractional crystallization; a similar observation was reported in Economos et al. (2009) in a 2 km wide southern lobe of the TIS composed mostly of eHD-pHD. All the studies cited above suggest at least km-scale magma bodies existed during the emplacement of the TIS, though how much mixing between them occurred at the level of emplacement is still debated.

Our study attempts to address the importance of these processes on a relatively limited scale, focusing on two small transects across the pHD-CP transitional zone which is approximately one kilometer wide and over 50 km long (Fig. 1). Our results summarized in the sections above require that (1) our samples of the pHD and CP solidified approximately 1.5 Myr apart; (2) magma mixing and/or prolonged magmatic growth contributed to the formation of some megacrysts in all three subunits; (3) there is little evidence in the zircon inclusion datasets that megacrysts in the CP originated in the pHD, despite evidence that TZ megacryst-hosted zircon ages are a mix of, or gradation between, the CP and pHD. Below, we use these constraints and previous work to discuss the lengthscales and duration over which magma mixing could have occurred across our transects.

To evaluate the potential scales of in situ mixing, we need to consider the size of magma bodies with a high enough melt fraction to mix, and the time scales of zircon crystallization. Our geochronological results from matrix zircon show that the youngest zircons in the pHD are approximately 1.1 Myr older than the oldest zircons (excluding what we interpret as xenocrysts) from the CP, and our final solidification ages for these units are over 1.5 Myr apart for both traverses (Fig. 2). This allows us to ask the question of whether or not the pHD and the CP had high melt fraction simultaneously where we sampled them, and therefore had the propensity to mix over several kilometers. In this hypothesis, it is required for the east traverse that the pHD reached its solidus before the CP reached zircon saturation 1.76 kilometers away. To quantify this a bit: if an estimate of zircon saturation in these magmas is 825˚C (Barnes et al., 2019) and the solidus 670°C (Johannes, 1984), our zircon data show that when the east-traverse pHD solidified, *if the CP was already emplaced*, then it would have needed to be at least 155˚C hotter and above zircon saturation. The CP would then have needed to remain above zircon saturation at the emplacement level for 1.1 Myr and subsequently reached the solidus 0.5 Myr after that, cooling at a rate of 310˚C/Myr.

This hypothesis can be addressed in part using existing thermal models for emplacement of the TIC. Memeti et al. (2010) presented U-Pb zircon ages and use a 2D thermal model to compare the cooling rates of a main magma chamber and four smaller magmatic lobes on the periphery of the TIS and concluded that the central plutonic body potentially formed magma chambers with melt present for > 1 Myr whereas the much smaller lobes largely crystallized in a few 100 kyr. Paterson et al. (2011) explored a wide range of growth scenarios and pulse shapes and sizes (from large diapirs to small dikes) and found that magma could be sustained at the emplacement level for over 1 Myr for several different scenarios. Schöpa and Annen (2013) developed a quasi-3D numerical model which emplaced the TIS as a series of sills of variable sizes and intrusion tempos. They found that melt rich conditions capable of mixing through convection (they used >50% melt) on the kilometer scale could be sustained for at most 115 kyr (Schöpa & Annen, 2013). All of these models, in addition to others not focussed on the TIS (e.g., Karakas et al., 2017; Gelman et al., 2013; Ratschbacher et al., 2018; Annen et al., 2006, 2008; Biggs and Annen 2019), have benefits and drawbacks, and can produce different estimates for the duration of melt present in a particular pulse or across the intrusive complex, depending on factors such as intrusion geometry and magma emplacement rate, the thermal state of a potentially transcrustal magmatic system, physical constants such as thermal conductivity, the relationship between temperature and crystallinity in magmas, etc. None of these models can account for magmatic processes proposed for the TIS such as re-melting of solidified in situ magmas (Barnes et al., 2011), erosion of older magmas (Žák & Paterson, 2005; Paterson et al., 2016), melt loss (Memeti et al., 2022), or hydrothermal circulation. What is important for our study, however, is to leverage what we can from these models given the time constraints imposed by the zircon dates given our higher sampling resolution compared to previous work. As best as we can understand, none of the models above are able to produce magmatic thermal gradients that would support the hypothesis that the pHD and CP were emplaced adjacently above (or below) zircon saturation and mixed at their contact to produce the TZ, then cooled to produce zircon dates in the pHD 1.5 Myr before the CP 1.76 km away. We therefore rule out a single large batch emplacement model, consistent with previous field, geochemical, and geochronologic work (Coleman et al., 2004; Memeti et al., 2010). We instead turn to a more dynamic set of emplacement mechanisms to explain mixing across the TZ.

K-feldspar megacrysts from all three subunits have significantly different core-included and matrix date populations (Table 1), and resolvable offsets between core and rim-included date populations (Fig. 3). Our data are consistent with TZ megacryst cores being derived from the same or similar magmas as the pHD samples, as proposed in Chambers et al. (2020). Our results are not consistent with megacrysts in the CP nucleating in the pHD, at least where we sampled it. In fact, only one of the 55 zircons we dated from CP megacrysts is of pHD age, strongly suggesting that the megacrysts we sampled from the CP did not nucleate within the pHD. The observation that zircon dates within the TZ are not bimodal (i.e., having only the ages represented in our CP or pHD samples, and nothing in between), but instead show a gradation between the CP and pHD ages, is also inconsistent with a model where CP magma intruded a fully solid pHD magma such that the TZ is gradational as a result of only assimilation (or crystal transport). Overall this indicates the TZ is the result of some combination of magma mixing (with or without assimilation or erosion of the pHD), with a maximum spatial extent of mixing across our transects of approximately the width of the TZ, under 2 km. The TZ serves as a gradational contact between the pHD and CP, but since the span of ages over this contact is large enough to preclude coeval crystallization, we consider it most likely that the TZ formed from a series of intruding increments of magma that initially mixed with pHD magmas and later each other (Fig. 6). It is not resolvable from our data how many of these increments formed the TZ or any other unit in the TIS, but the differences in matrix solidification ages from TIC11 compared to the other TZ sampling locations suggests that at least final crystallization in the TZ from zircon saturation to the solidus occurred at slightly different times along strike of the TZ.

Despite our conclusion that magma mixing across the TZ was limited to approximately its width, we find four ante- or xenocrystic zircons preserved in the CP megacrysts, which is consistent with earlier work indicating some limited antecrystic and xenocrystic zircons in other CP dated samples (Memeti et al., 2010; Paterson et al., 2016). However, the total number of pre- ca. 88 Ma antecrystic zircons has drastically decreased in the CP in comparison to that in the pHD and transition zone (Fig. 2). One possible mechanism to explain zircon inheritance (as well as other minerals) in the CP was observed in Sawmill Canyon, where it was suggested based on textural and geochemical data that younger CP magma cross-cut and eroded older units such as the KC and eHD (Paterson et al., 2008). This is consistent with some interpretations of the spatial distribution of the units of the TIS (Fig. 1) which argue that that each portion of the pHD-CP transition was once continuous across the interior of the TIS prior to being intruded by subsequent pulses of the next younger unit (Paterson et al., 2016). Additionally, the observed inherited zircon could be incorporated prior during magma ascent, as inferred to be an important process for other antecrystic minerals. Further understanding the controls on zircon inheritance could be aided by more detailed observations of zircon textures, in addition to Ti-in-zircon crystallization temperatures to better constrain resorption histories and zircon saturation windows. Such studies may also lead to a better understanding of how much magma composition is controlled through source variability versus mixing, fractional crystallization and assimilation during ascent, emplacement, and final solidification (Coleman et al., 2012; Economos et al., 2009; Gray et al., 2008; Paterson et al., 2016).

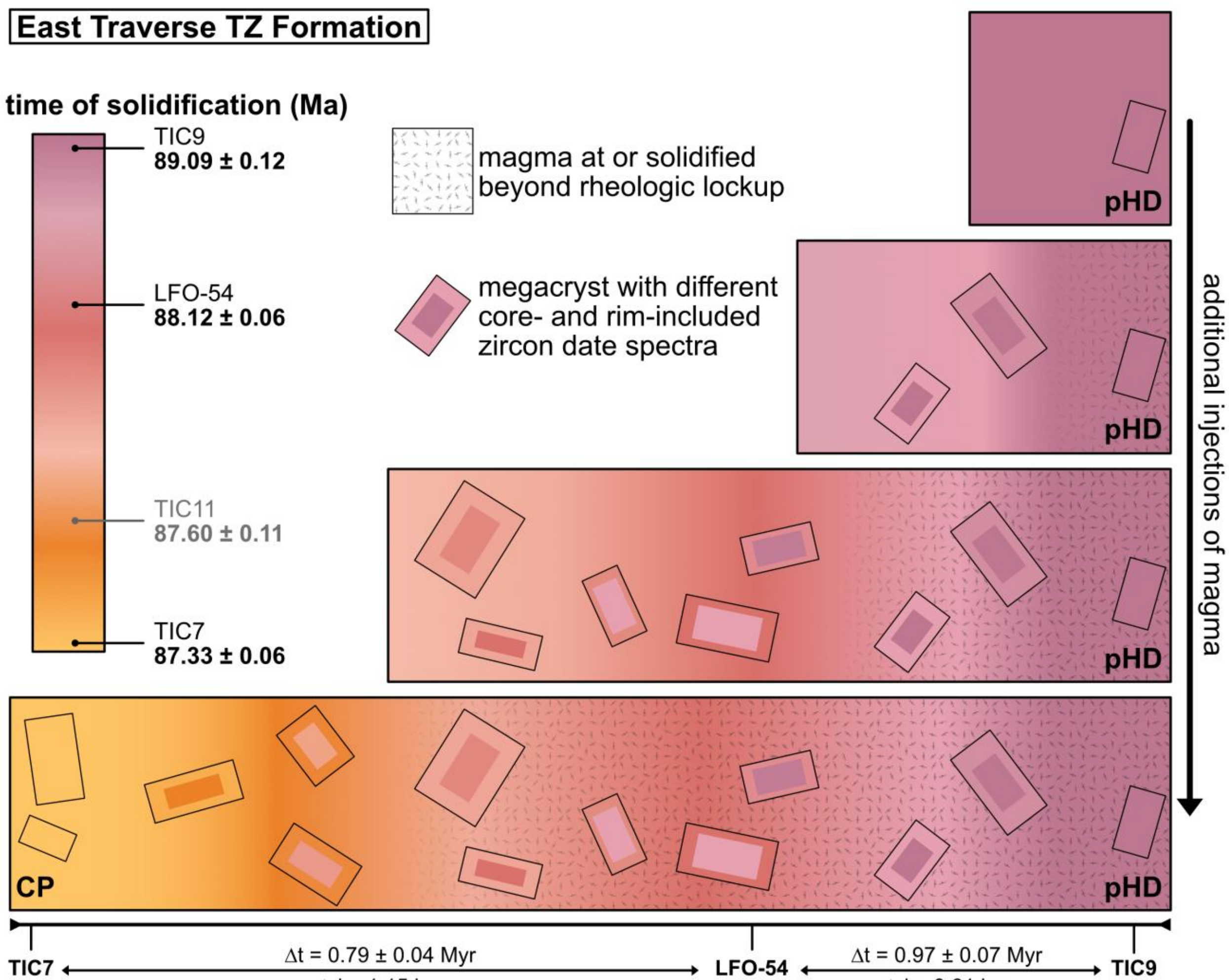

Figure 6 Schematic visualization of the formation of the TZ across an approximately linear subset of the east traverse. Color gradients represent potential co-magmatic mixing or crystal erosion and transfer relationships between temporally distinct pulses of magma. The solidification age of TIC11 is also included in the color gradient key for additional context, but that sample site falls outside the approximately linear transect formed by the other three shown Four pulses are shown making up the TZ here as an example, but the true number of pulses is not resolvable from our results. Δt is the time between the modeled final matrix solidification ages of the samples and Δd is the distance between the sampling sites. Megacrysts are not drawn to scale.

6 Conclusions

New U-Pb ages from zircons included in TIS megacrysts and matrix samples from the pHD, TZ, and CP support previous interpretations (Chambers et al., 2020) that the TZ represents a region of mixing. However, this mixing signal is weaker outside the TZ, suggesting the spatial extent of mixing or magmatic erosion and crystal transfer at a given point in time was limited to 2 km at most (the approximate width of the TZ) or was erased by subsequent intrusion of CP magmas. Further, matrix ages preclude the pHD and CP from being melt-rich at the same time where we sampled them. Our results within the context of studies from other plutonic settings add to evidence of small-scale mixing and hybridization.

Acknowledgments

The authors declare no conflicts of interest relevant to this study. This work was funded by the US National Science Foundation (awards #2223333, #2223332, #15550935, and #1624854). We thank the University of Texas at Austin Computed Tomography lab (UTCT) for generating CT scans. We thank Michael P. Eddy and Melissa Chambers for contributing zircon U-Pb dates for the megacryst sample LFO-51. We are grateful to Dawid Szymanowski and Stefania Gili for support with U-Pb and zircon trace element measurements, respectively. Thanks to Scott Paterson for guidance and insight during sampling, and to Joshua Rosera for valuable feedback during the development of the modified K-S test. We also thank editor Paul Asimow, our associate editor, two anonymous reviewers and Carl Beno for their thoughtful reviews. Thanks to the National Park Service for granting sampling permits for our work in Yosemite National Park. Any use of trade, firm, or product names is for descriptive purposes only and does not imply endorsement by the U.S. Government.

Open Research

All data presented are available at Watts et al. (2024).

References

Ackerson, M.R., Mysen, B.O., Tailby, N.D., Watson, E.B., 2018. Low-temperature crystallization of granites and the implications for crustal magmatism. *Nature* 559, 94–97. https://doi.org/10.1038/s41586-018-0264-2

Ague, J.J., Brimhall, G.H., 1988. Magmatic arc asymmetry and distribution of anomalous plutonic belts in the batholiths of California: Effects of assimilation, crustal thickness, and depth of crystallization. *GSA Bulletin* 100, 912–927. https://doi.org/10.1130/0016-7606(1988)100<0912:MAAADO>2.3.CO;2

Annen, C., Blundy, J. D., & Sparks, R. S. J. (2006). The Genesis of Intermediate and Silicic Magmas in Deep Crustal Hot Zones. *Journal of Petrology*, 47(3), 505–539. https://doi.org/10.1093/petrology/egi084

Annen, C., Pichavant, M., Bachmann, O., & Burgisser, A. (2008). Conditions for the growth of a long-lived shallow crustal magma chamber below Mount Pelee volcano (Martinique, Lesser Antilles Arc). *Journal of Geophysical Research: Solid Earth*, 113(B7). https://doi.org/10.1029/2007JB005049

Barboni, M., Annen, C., Schoene, B., 2015. Evaluating the construction and evolution of upper crustal magma reservoirs with coupled U/Pb zircon geochronology and thermal modeling: A case study from the Mt. Capanne pluton (Elba, Italy). *Earth Planet Sci Lett* 432, 436–448. https://doi.org/10.1016/j.epsl.2015.09.043

Barboni, M., Schoene, B., 2014. Short eruption window revealed by absolute crystal growth rates in a granitic magma. Nat Geosci 7, 524–528. https://doi.org/10.1038/ngeo2185

Barnes, C.G., Memmeti, V., Coint, N., 2016. Deciphering magmatic processes in calc-alkaline plutons using trace element zoning in hornblende. *American Mineralogist* 101, 328–342. https://doi.org/10.2138/AM-2016-5383

Barnes, C.G., Werts, K., Memeti, V., Ardill, K., 2019. Most Granitoid Rocks are Cumulates: Deductions from Hornblende Compositions and Zircon Saturation. *Journal of Petrology* 60, 2227–2240. https://doi.org/10.1093/PETROLOGY/EGAA008

Barnes, C. G., Werts, K., Memeti, V., Paterson, S. R., & Bremer, R. (2021). A tale of five enclaves: Mineral perspectives on origins of mafic enclaves in the Tuolumne Intrusive Complex. *Geosphere*, *17*(2), 352–374. https://doi.org/10.1130/GES02233.1

Bartley, J.M., Coleman, D.S., Glazner, A.F., 2006. Incremental pluton emplacement by magmatic crack-seal. *Earth Environ Sci Trans R Soc Edinb* 97, 383–396. https://doi.org/10.1017/S0263593300001528

Bateman, P.C., 1992. Plutonism in the central part of the Sierra Nevada Batholith, California. *United States Geological Survey Professional Paper* 1483, 1–186. https://doi.org/10.3133/PP1483

Bateman, P.C., Chappell, B.W., 1979. Crystallization, fractionation, and solidification of the Tuolumne Intrusive Series, Yosemite National Park, California. *GSA Bulletin* 90, 465–482.

Bateman, P.C., Kistler, R.W., Peck, D.L., Busacca, A., 1983. Geologic map of the Tuolumne Meadows quadrangle, Yosemite National Park, California. Geologic Quadrangle. https://doi.org/10.3133/GQ1570

Biggs, J., & Annen, C. (2019). The lateral growth and coalescence of magma systems. *Philosophical Transactions of the Royal Society A*, 377(2139). https://doi.org/10.1098/RSTA.2018.0005

Brophy, J.G., Ota, T., Kunihro, T., Tsujimori, T., Nakamura, E., 2011. In situ ion-microprobe determination of trace element partition coefficients for hornblende, plagioclase, orthopyroxene, and apatite in equilibrium with natural rhyolitic glass, Little Glass Mountain Rhyolite, California. *American Mineralogist* 96, 1838–1850. https://doi.org/10.2138/AM.2011.3857

Burgess, S.D., Miller, J.S., 2008. Construction, solidification and internal differentiation of a large felsic arc pluton: Cathedral Peak granodiorite, Sierra Nevada Batholith. *Geol Soc Spec Publ* 304, 203–233. https://doi.org/https://doi-org/10.1144/SP304.11

Chambers, M., Memeti, V., Eddy, M.P., Schoene, B., 2020. Half a million years of magmatic history recorded in a K-feldspar megacryst of the tuolumne intrusive complex, California, USA. *Geology* 48, 400–404. https://doi.org/10.1130/G46873.1

Claiborne, L.L., Miller, C.F., Walker, B.A., Wooden, J.L., Mazdab, F.K., Bea, F., 2006. Tracking magmatic processes through Zr/Hf ratios in rocks and Hf and Ti zoning in zircons: An example from the Spirit Mountain batholith, Nevada. Mineral Mag 70, 517–543. https://doi.org/10.1180/0026461067050348

Coleman, D.S., Bartley, J.M., Glazner, A.F., Pardue, M.J., 2012. Is chemical zonation in plutonic rocks driven by changes in source magma composition or shallow-crustal differentiation? Geosphere 8, 1568–1587. https://doi.org/10.1130/GES00798.1

Coleman, D.S., Gray, W., Glazner, A.F., 2004. Rethinking the emplacement and evolution of zoned plutons: Geochronologic evidence for incremental assembly of the Tuolumne Intrusive Suite, California. *Geology* 32, 433–436. https://doi.org/10.1130/G20220.1

Condon, D., Schoene, B., Schmitz, M., Schaltegger, U., Ickert, R., Amelin, Y., Augland, L.E., Chamberlain, K., Coleman, D.S., Connelly, J.N., Corfu, F., Crowley, J.L., Davies, J.H.F.L., Denyszyn, S.W., Eddy, M.P., Heaman, L.M., Huyskens, M.H., Gaynor, S.P., Kamo, S., Kasbohm, Keller, C.B., MacLennan, S.A., McLean, N.M., Noble, S., Ovtcharova, M., Paul, A., Ramezani, J., Rioux, M., Sahy, D., Scoates, J., Szymanowski, D., Tapster, S., Tichomirowa, M., Wall, C., Wotzlaw, J.F., Yang, C., Yin, Q.Z., 2024, Recommendations for the Reporting and Interpretation of Isotope Dilution U-Pb Geochronological Information: Geological Society of America Bulletin, v. 136, p. 4233-4251.

Cox, R.A., Dempster, T.J., Bell, B.R., Rogers, G., 1996. Crystallization of the Shap Granite: Evidence from zoned K-feldspar megacrysts. *J Geol Soc London* 153, 625–635. https://doi.org/10.1144/GSJGS.153.4.0625

Curry, A., Gaynor, S.P., Davies, J.H.F.L., Ovtcharova, M., Simpson, G., Caricchi, L., 2021. Timescales and thermal evolution of large silicic magma reservoirs during an ignimbrite flare-up: perspectives from zircon. *Contributions to Mineralogy and Petrology* 2021 176:12 176, 1–27. https://doi.org/10.1007/S00410-021-01862-W

Economos, R. C., Memeti, V., Paterson, S. R., Miller, J. S., Erdmann, S., & Žák, J. (2009). Causes of compositional diversity in a lobe of the Half Dome granodiorite, Tuolumne Batholith, Central Sierra Nevada, California. *Earth and Environmental Science Transactions of the Royal Society of Edinburgh*, 100, 173–183. https://doi.org/10.1017/S1755691009016065

Eddy, M.P., Pamukçu, A., Schoene, B., Steiner-Leach, T., Bell, E.A., 2022. Constraints on the timescales and processes that led to high-SiO2 rhyolite production in the Searchlight pluton, Nevada, USA. *Geosphere* 18. https://doi.org/10.1130/GES02439.1

Farina, F., Dini, A., Innocenti, F., Rocchi, S., Westerman, D.S., 2010. Rapid incremental assembly of the Monte Capanne pluton (Elba Island, Tuscany) by downward stacking of magma sheets. *GSA Bulletin* 122, 1463–1479. https://doi.org/10.1130/B30112.1

Farina, F., Stevens, G., Gerdes, A., Frei, D., 2014. Small-scale Hf isotopic variability in the Peninsula pluton (South Africa): the processes that control inheritance of source 176Hf/177Hf diversity in S-type granites. *Contributions to Mineralogy and Petrology* 168, 1–18. https://doi.org/10.1007/s00410-014-1065-8

Gagnevin, D., Daly, J.S., Poli, G., Morgan, D., 2005. Microchemical and Sr Isotopic Investigation of Zoned K-feldspar Megacrysts: Insights into the Petrogenesis of a Granitic System and Disequilibrium Crystal Growth. *Journal of Petrology* 46, 1689–1724. https://doi.org/10.1093/PETROLOGY/EGI031

Gaynor, S.P., Coleman, D.S., Rosera, J.M., Tappa, M.J., 2019. Geochronology of a Bouguer Gravity Low. *J Geophys Res Solid Earth* 124, 2457–2468. https://doi.org/10.1029/2018JB015923

Gaynor, S.P., Smith, T.M., Schaltegger, U., 2023. Tracing magmatic genesis and evolution through single zircon crystals from successive supereruptions from the Socorro Caldera Complex, USA. *Earth Planet Sci Lett* 616, 118236. https://doi.org/10.1016/J.EPSL.2023.118236

Gelman, S.E., Gutiérrez, F.J., Bachmann, O., 2013. On the longevity of large upper crustal silicic magma reservoirs. *Geology* 41, 759–762. https://doi.org/10.1130/G34241.1

Glazner, A. F., Bartley, J. M., Coleman, D. S., Gray, W., & Taylor, R. Z. (2004). Are plutons assembled over millions of years by amalgamation from small magma chambers? *GSA Today*, *14*(4/5). https://doi.org/10.1130/1052-5173(2004)014<0004:APAOMO>2.0.CO;2

Glazner, A.F., Johnson, B.R., 2013. Late crystallization of K-feldspar and the paradox of megacrystic granites. *Contributions to Mineralogy and Petrology* 166, 777–799. https://doi.org/10.1007/s00410-013-0914-1

Gordon, C., Wallis, D., 2024. Resolving the "megacryst paradox": Feldspar orientation relationships record crystal mobility in granites. *Geology* 52, 712–716. https://doi.org/10.1130/G52045.1

Gray, W., Glazner, A.F., Coleman, D.S., Bartley, J.M., 2008. Long-term geochemical variability of the Late Cretaceous Tuolumne Intrusive Suite, central Sierra Nevada, California. *Geol Soc Spec Publ* 304, 183–201. https://doi.org/10.1144/SP304.10

Horsman, E., Morgan, S., De Saint-Blanquat, M., Habert, G., Nugent, A., Hunter, R.A., Tikoff, B., 2009. Emplacement and assembly of shallow intrusions from multiple magma pulses, Henry Mountains, Utah. *Earth Environ Sci Trans R Soc Edinb* 100, 117–132. https://doi.org/10.1017/S1755691009016089

Johannes, W., 1984. Beginning of melting in the granite system Qz-Or-Ab-An-H2O. *Contributions to Mineralogy and Petrology* 86, 264–273. https://doi.org/10.1007/BF00373672/METRICS

Johnson, B.R., Glazner, A.F., 2010. Formation of K-feldspar megacrysts in granodioritic plutons by thermal cycling and late-stage textural coarsening. *Contributions to Mineralogy and Petrology* 159, 599–619. https://doi.org/10.1007/s00410-009-0444-z

Karakas, O., Dufek, J., Mangan, M. T., Wright, H. M., & Bachmann, O. (2017). Thermal and petrologic constraints on lower crustal melt accumulation under the Salton Sea Geothermal Field. *Earth and Planetary Science Letters*, *467*, 10–17. https://doi.org/10.1016/j.epsl.2017.02.027

Keller, C.B., Schoene, B., Samperton, K.M., 2018. A stochastic sampling approach to zircon eruption age interpretation. *Geochemical Perspectives Letters* (Online) 8, 31–35. https://doi.org/10.7185/geochemlet.1826

Kistler, R.W., Chappell, B.W., Peck, D.L., Bateman, P.C., 1986. Isotopic variation in the Tuolumne Intrusive Suite, central Sierra Nevada, California. *Contributions to Mineralogy and Petrology* 94, 205–220. https://doi.org/10.1007/BF00592937

Kistler, R.W., Fleck, R.J., 1994. Field guide for a transect of the central Sierra Nevada, California; geochronology and isotope geology. Open-File Report. https://doi.org/10.3133/OFR94267

Klein, B.Z., Eddy, M.P., 2024. What's in an age? Calculation and interpretation of ages and durations from U-Pb zircon geochronology of igneous rocks. *GSA Bulletin* 136, 93–109. https://doi.org/10.1130/B36686.1

Lackey, J.S., Valley, J.W., Saleeby, J.B., 2005. Supracrustal input to magmas in the deep crust of Sierra Nevada batholith: Evidence from high-δ18O zircon. *Earth Planet Sci Lett* 235, 315–330. https://doi.org/10.1016/J.EPSL.2005.04.003

Mahood, G., Hildreth, W., 1983. Large partition coefficients for trace elements in high-silica rhyolites. *Geochim Cosmochim Acta* 41, 11–30. https://doi.org/10.1016/0016-7037(83)90087-X

Massey, F.J., 1951. The Kolmogorov-Smirnov Test for Goodness of Fit. *J Am Stat Assoc* 46, 68–78. https://doi.org/10.1080/01621459.1951.10500769

Matzel, J.E.P., Bowring, S.A., Miller, R.B., 2006. Time scales of pluton construction at differing crustal levels: Examples from the Mount Stuart and Tenpeak intrusions, North Cascades, Washington. *GSA Bulletin* 118, 1412–1430. https://doi.org/10.1130/B25923.1

McNulty, B.A., Tong, W., Tobisch, O.T., 1996. Assembly of a dike-fed magma chamber: The Jackass Lakes pluton, central Sierra Nevada, California. *GSA Bulletin* 108, 926–940.

Memeti, V., Paterson, S., Matzel, J., Mundil, R., Okaya, D., 2010. Magmatic lobes as "snapshots" of magma chamber growth and evolution in large, composite batholiths: An example from the Tuolumne intrusion, Sierra Nevada, California. *Bulletin of the Geological Society of America* 122, 1912–1931. https://doi.org/10.1130/B30004.1

Memeti, V., Paterson, S.R., Mundil, R., 2022. Coupled magmatic and host rock processes during the initiation of the Tuolumne Intrusive Complex, Sierra Nevada, California, USA: A transition from ephemeral sheets to long-lived, active magma mushes. *GSA Bulletin* 134, 1347–1374. https://doi.org/10.1130/B35871.1

Michel, J., Baumgartner, L., Putlitz, B., Schaltegger, U., Ovtcharova, M., 2008. Incremental growth of the Patagonian Torres del Paine laccolith over 90 k.y. *Geology* 36, 459–462. https://doi.org/10.1130/G24546A.1

Miller, J. S., Matzel, J. E. P., Miller, C. F., Burgess, S. D., & Miller, R. B. (2007). Zircon growth and recycling during the assembly of large, composite arc plutons. *Journal of Volcanology and Geothermal Research*, *167*(1–4), 282–299. https://doi.org/10.1016/J.JVOLGEORES.2007.04.019

Moore, J.G., Sisson, T.W., 2008. Igneous phenocrystic origin of K-feldspar megacrysts in granitic rocks from the Sierra Nevada batholith. *Geosphere* 4, 387–400. https://doi.org/10.1130/GES00146.1

Oppenheim, L.F., Memeti, V., Barnes, C.G., Chambers, M., Krause, J., Esposito, R., 2021. Feldspar recycling across magma mush bodies during the voluminous Half Dome and Cathedral Peak stages of the Tuolumne intrusive complex, Yosemite National Park, California, USA. *Geosphere* 17, 322–351. https://doi.org/10.1130/GES02286.1

Paterson, S. R., Žák, J., & Janoušek, V. (2008). Growth of complex sheeted zones during recycling of older magmatic units into younger: Sawmill Canyon area, Tuolumne batholith, Sierra Nevada, California. *Journal of Volcanology and Geothermal Research*, *177*(2), 457–484. https://doi.org/10.1016/j.jvolgeores.2008.06.024

Paterson, S., Memeti, V., Mundil, R., Žák, J., 2016. Repeated, multiscale, magmatic erosion and recycling in an upper-crustal pluton: Implications for magma chamber dynamics and magma volume estimates. *American Mineralogist* 101, 2176–2198. https://doi.org/10.2138/am-2016-5576

Paterson, S.R., Okaya, D., Memeti, V., Economos, R., Miller, R.B., 2011. Magma addition and flux calculations of incrementally constructed magma chambers in continental margin arcs: Combined field, geochronologic, and thermal modeling studies. *Geosphere* 7, 1439–1468. https://doi.org/10.1130/GES00696.1

Ratschbacher, B.C., Brenhin Keller, C., Schoene, B., Paterson, S.R., Lawford Anderson, J., Okaya, D., Putirka, K., Lippoldt, R., 2018. A New Workflow to Assess Emplacement Duration and Melt Residence Time of Compositionally Diverse Magmas Emplaced in a Sub-volcanic Reservoir. *Journal of Petrology* 59, 1787–1809. https://doi.org/10.1093/PETROLOGY/EGY079

Rout, S.S., Blum-Oeste, M., Wörner, G., 2021. Long-term temperature cycling in a shallow magma reservoir: insights from sanidine megacrysts at Taápaca volcano, Central Andes. *Journal of Petrology*. https://doi.org/10.1093/PETROLOGY/EGAB010

Rout, S. S., Wörner, G., Wegner, W., & Singer, B. S. (2024). Heat pulse–dominated magmatic storage: The 33 ka dacite dome eruption at Taápaca volcano (Central Andes). *Geology*, 52(9), 683–688. https://doi.org/10.1130/G52173.1

Rubatto, D., Hermann, J., 2007. Experimental zircon/melt and zircon/garnet trace element partitioning and implications for the geochronology of crustal rocks. *Chem Geol.* https://doi.org/10.1016/j.chemgeo.2007.01.027

Samperton, K.M., Schoene, B., Cottle, J.M., Brenhin Keller, C., Crowley, J.L., Schmitz, M.D., 2015. Magma emplacement, differentiation and cooling in the middle crust: Integrated zircon geochronological-geochemical constraints from the Bergell Intrusion, Central Alps. *Chem Geol* 417, 322–340. https://doi.org/10.1016/j.chemgeo.2015.10.024

Schaltegger, U., Brack, P., Ovtcharova, M., Peytcheva, I., Schoene, B., Stracke, A., Marocchi, M., Bargossi, G.M., 2009. Zircon and titanite recording 1.5 million years of magma accretion, crystallization and initial cooling in a composite pluton (southern Adamello batholith, northern Italy). *Earth Planet Sci Lett* 286, 208–218. https://doi.org/10.1016/J.EPSL.2009.06.028

Schaltegger, U., Ovtcharova, M., Gaynor, S.P., Schoene, B., Wotzlaw, J.F., Davies, J.F.H.L., Farina, F., Greber, N.D., Szymanowski, D., Chelle-Michou, C., 2021. Long-term repeatability and interlaboratory reproducibility of high-precision ID-TIMS U–Pb geochronology. *J Anal At Spectrom* 36, 1466–1477. https://doi.org/10.1039/D1JA00116G

Schoene, B., Latkoczy, C., Schaltegger, U., Günther, D., 2010. A new method integrating high-precision U-Pb geochronology with zircon trace element analysis (U-Pb TIMS-TEA). *Geochim Cosmochim Acta* 74, 7144–7159. https://doi.org/10.1016/j.gca.2010.09.016

Schoene, B., Schaltegger, U., Brack, P., Latkoczy, C., Stracke, A., Günther, D., 2012. Rates of magma differentiation and emplacement in a ballooning pluton recorded by U–Pb TIMS-TEA, Adamello batholith, Italy. *Earth Planet Sci Lett* 355–356, 162–173. https://doi.org/10.1016/J.EPSL.2012.08.019

Schöpa, A., Annen, C., 2013. The effects of magma flux variations on the formation and lifetime of large silicic magma chambers. *J Geophys Res Solid Earth* 118, 926–942. https://doi.org/10.1002/JGRB.50127

Shea, E.K., Miller, J.S., Miller, R.B., Bowring, S.A., Sullivan, K.M., 2016. Growth and maturation of a mid- to shallow-crustal intrusive complex, North Cascades, Washington. *Geosphere* 12, 1489–1516. https://doi.org/10.1130/GES01290.1

Tappa, Michael J, Coleman, Drew S, Mills, Ryan D, Samperton, Kyle M, Tappa, M J, Coleman, D S, Mills, R D, Samperton, K M, 2011. The plutonic record of a silicic ignimbrite from the Latir volcanic field, New Mexico. *Geochemistry, Geophysics, Geosystems* 12, 10011. https://doi.org/10.1029/2011GC003700

Tapster, S., Condon, D.J., Naden, J., Noble, S.R., Petterson, M.G., Roberts, N.M.W., Saunders, A.D., Smith, D.J., 2016. Rapid thermal rejuvenation of high-crystallinity magma linked to porphyry copper deposit formation; evidence from the Koloula Porphyry Prospect, Solomon Islands. *Earth Planet Sci Lett* 442, 206–217. https://doi.org/10.1016/J.EPSL.2016.02.046

Tavazzani, L., Wotzlaw, J.F., Economos, R., Sinigoi, S., Demarchi, G., Szymanowski, D., Laurent, O., Bachmann, O., Chelle-Michou, C., 2023. High-precision zircon age spectra record the dynamics and evolution of large open-system silicic magma reservoirs. *Earth Planet Sci Lett* 623, 118432. https://doi.org/10.1016/J.EPSL.2023.118432

Vernon, R.H., 1986. K-feldspar megacrysts in granites — Phenocrysts, not porphyroblasts. *Earth Sci Rev* 23, 1–63. https://doi.org/10.1016/0012-8252(86)90003-6

Wallace, G.S., Bergantz, G.W., 2002. Wavelet-based correlation (WBC) of zoned crystal populations and magma mixing. *Earth Planet Sci Lett* 202, 133–145. https://doi.org/10.1016/S0012-821X(02)00762-8

Watts, E., Ye, J., Gaynor, S., Memeti, V., & Schoene, B. (2024). Data from 'Insights from Megacryst-Included Zircon Dates on the Spatial Extent of Magma Mixing in the Tuolumne Intrusive Complex, California, USA' [Data set]. Zenodo. https://doi.org/10.5281/zenodo.14497667

Wilkinson, J.J., 2013. Triggers for the formation of porphyry ore deposits in magmatic arcs. *Nature Geoscience* 2013 6:11 6, 917–925. https://doi.org/10.1038/NGEO1940

Žák, J., Paterson, S.R., 2010. Magmatic erosion of the solidification front during reintrusion: The eastern margin of the Tuolumne batholith, Sierra Nevada, California. *International Journal of Earth Sciences* 99, 801–812. https://doi.org/10.1007/S00531-009-0423-7/FIGURES/10

Žák, J., Paterson, S.R., 2005. Characteristics of internal contacts in the Tuolumne Batholith, central Sierra Nevada, California (USA): Implications for episodic emplacement and physical processes in a continental arc magma chamber. *GSA Bulletin* 117, 1242–1255. https://doi.org/10.1130/B25558.1

Figure1.

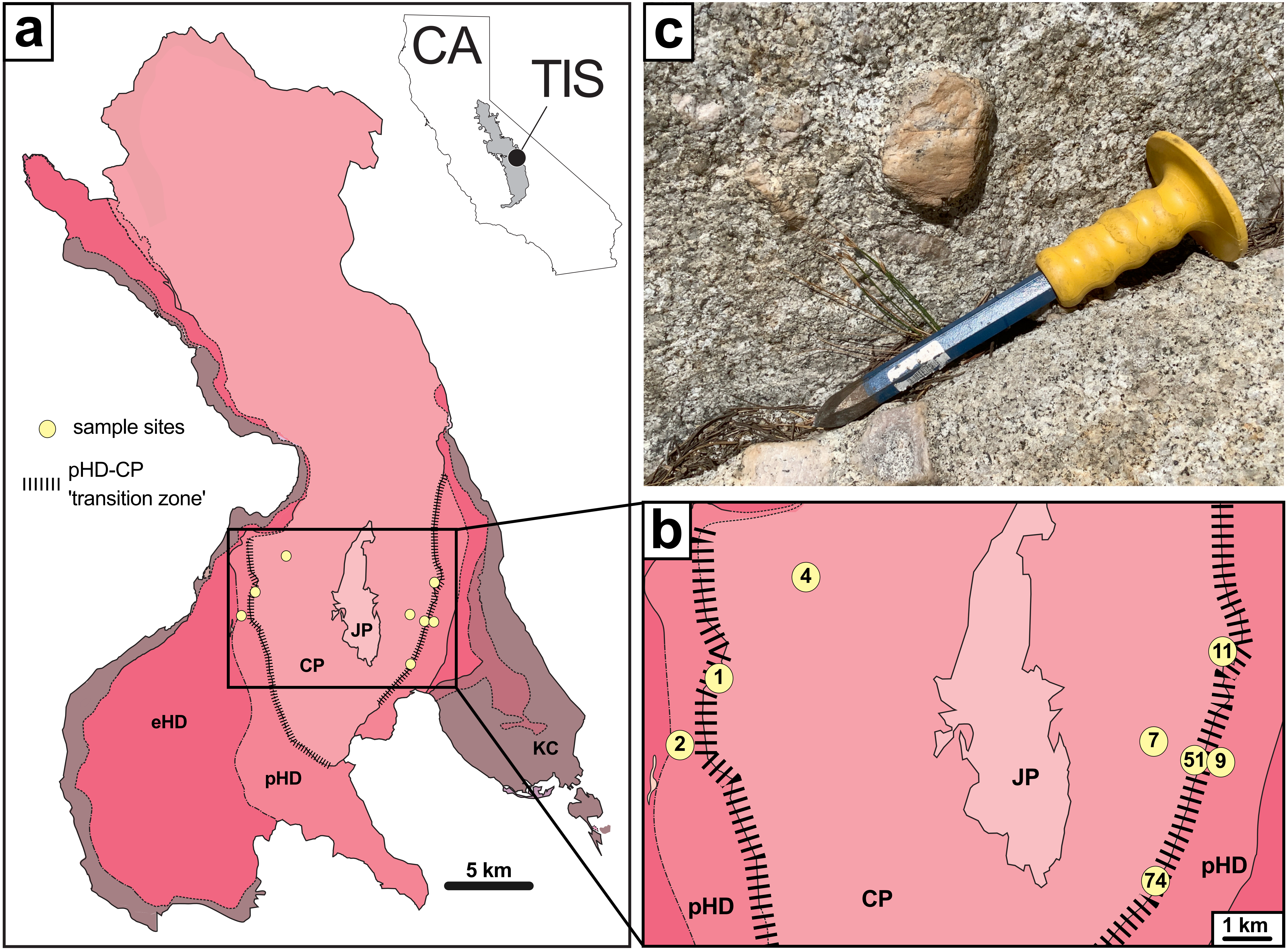

a
CA
TIS
sample sites
pHD-CP
'transition zone'
JP
CP
eHD
pHD
KC
5 km
c
b
4
1
2
11
7
51
9
74
JP
CP
pHD
pHD
1 km

Figure2.

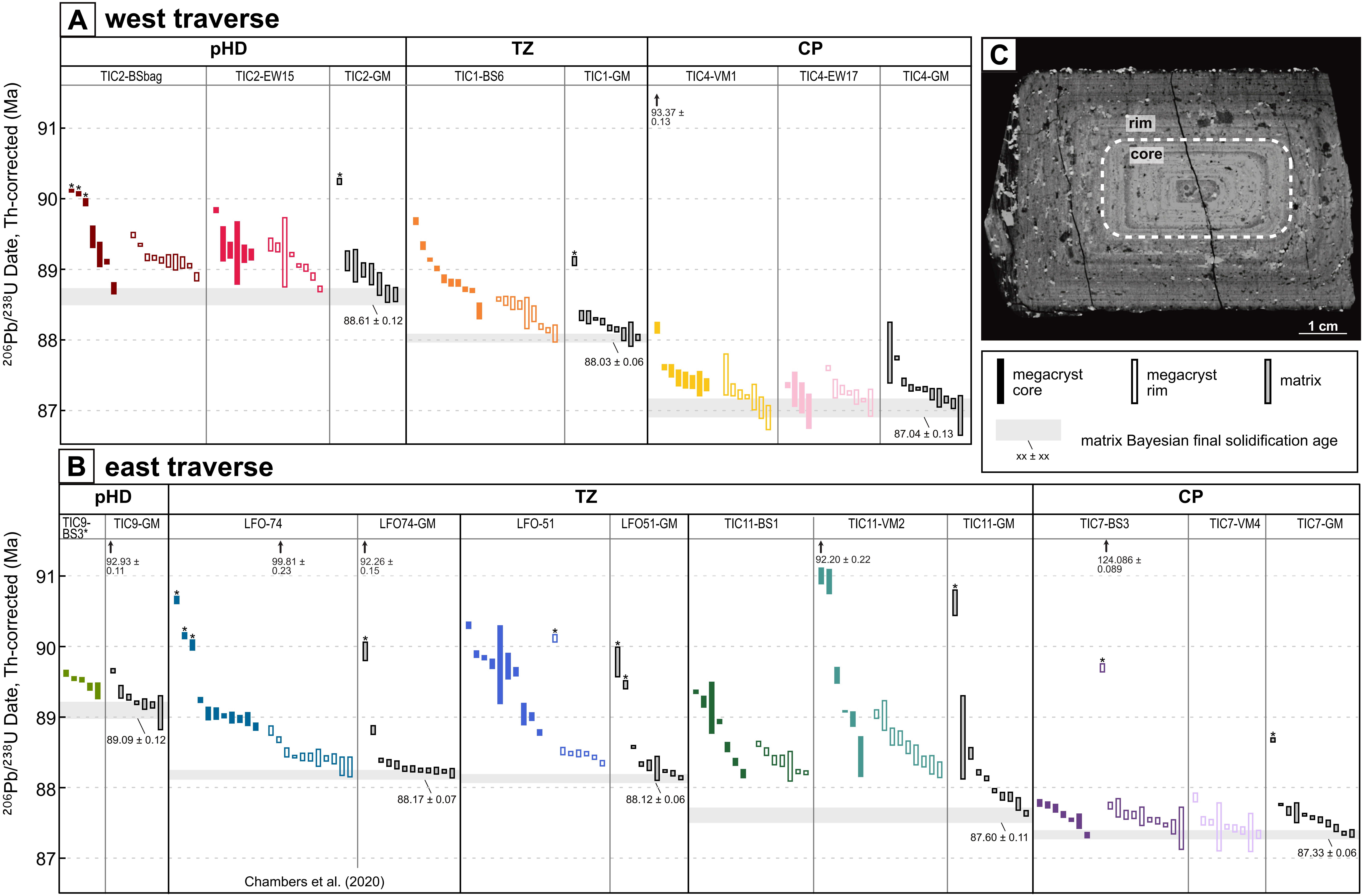

A west traverse
pHD
TZ
CP
TIC2-BSbag
TIC2-EW15
TIC2-GM
TIC1-BS6
TIC1-GM
TIC4-VM1
TIC4-EW17
TIC4-GM
93.37 ± 0.13
88.61 ± 0.12
88.03 ± 0.06
87.04 ± 0.13
C
rim
core
1 cm
megacryst core
megacryst rim
matrix
matrix Bayesian final solidification age
xx ± xx
B east traverse
TIC9-BS3*
TIC9-GM
LFO-74
LFO74-GM
LFO-51
LFO51-GM
TIC11-BS1
TIC11-VM2
TIC11-GM
TIC7-BS3
TIC7-VM4
TIC7-GM
92.93 ± 0.11
99.81 ± 0.23
92.26 ± 0.15
92.20 ± 0.22
124.086 ± 0.089
89.09 ± 0.12
88.17 ± 0.07
88.12 ± 0.06
87.60 ± 0.11
87.33 ± 0.06
Chambers et al. (2020)
206Pb/238U Date, Th-corrected (Ma)

Figure3.

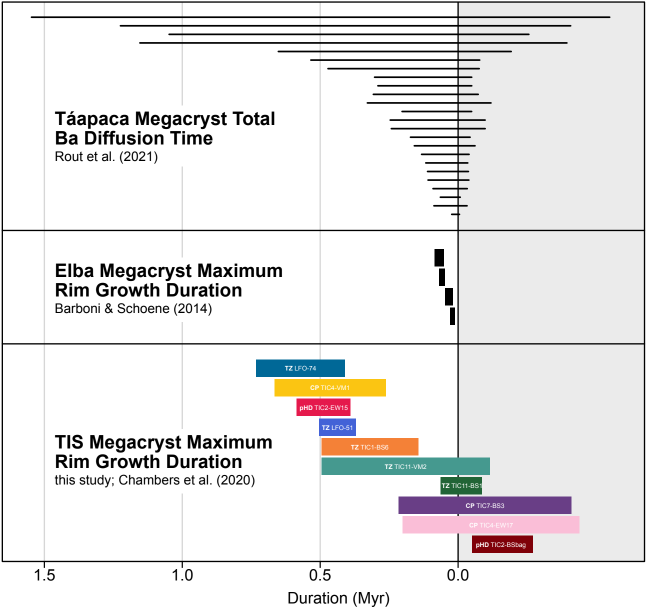
Táapaca Megacryst Total Ba Diffusion Time
Rout et al. (2021)
Elba Megacryst Maximum Rim Growth Duration
Barboni & Schoene (2014)
TIS Megacryst Maximum Rim Growth Duration
this study; Chambers et al. (2020)
TZ LFO-74
CP TIC4-VM1
pHD TIC2-EW15
TZ LFO-51
TZ TIC1-BS6
TZ TIC11-VM2
TZ TIC11-BS1
CP TIC7-BS3
CP TIC4-EW17
pHD TIC2-BSbag
1.5
1.0
0.5
0.0
Duration (Myr)

Figure4.

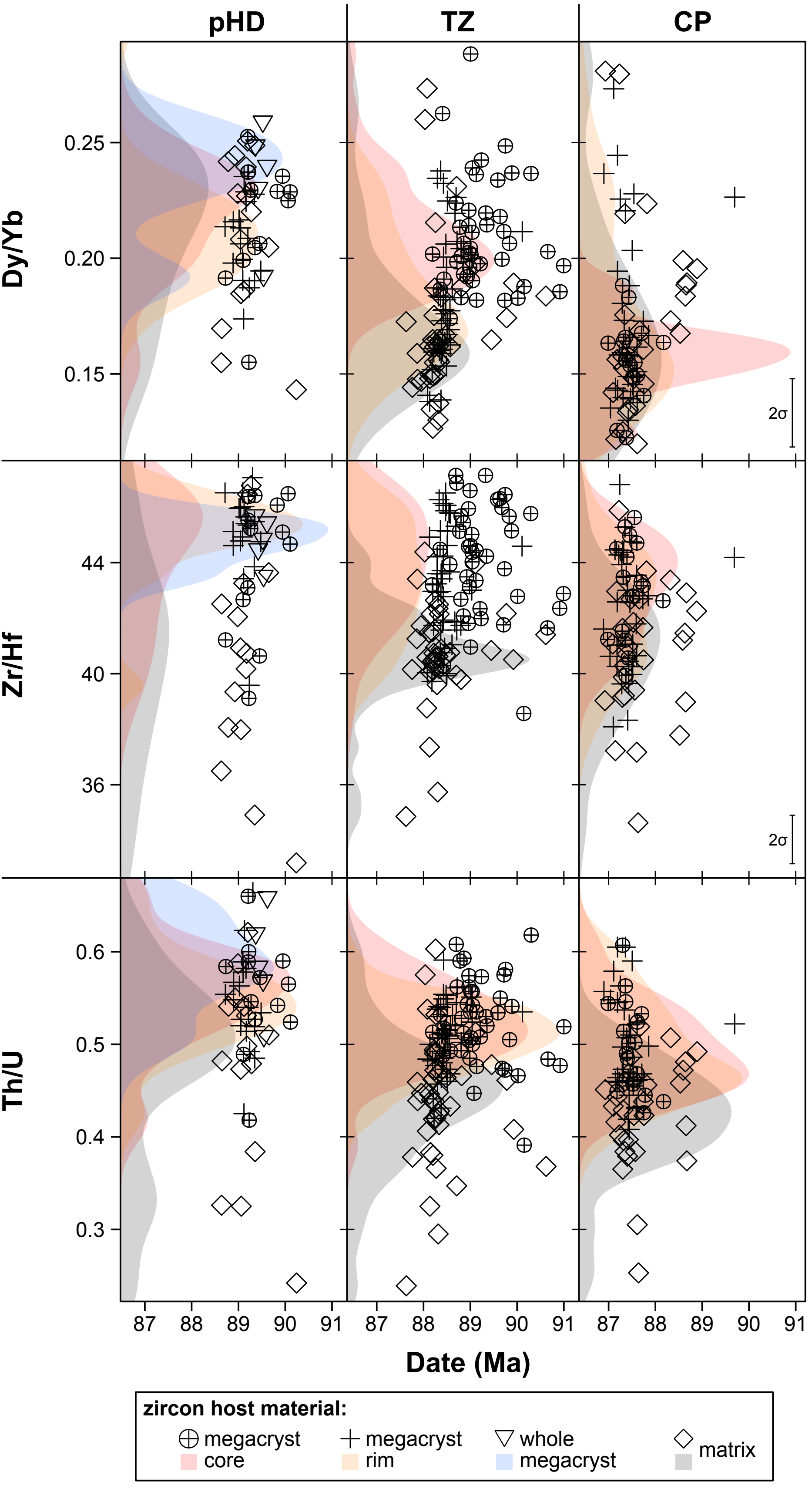

pHD
TZ
CP
Dy/Yb
0.25
0.20
0.15
2σ
Zr/Hf
44
40
36
2σ
Th/U
0.6
0.5
0.4
0.3
87
88
89
90
91
Date (Ma)
zircon host material:
megacryst core
megacryst rim
whole megacryst
matrix

Figure5.

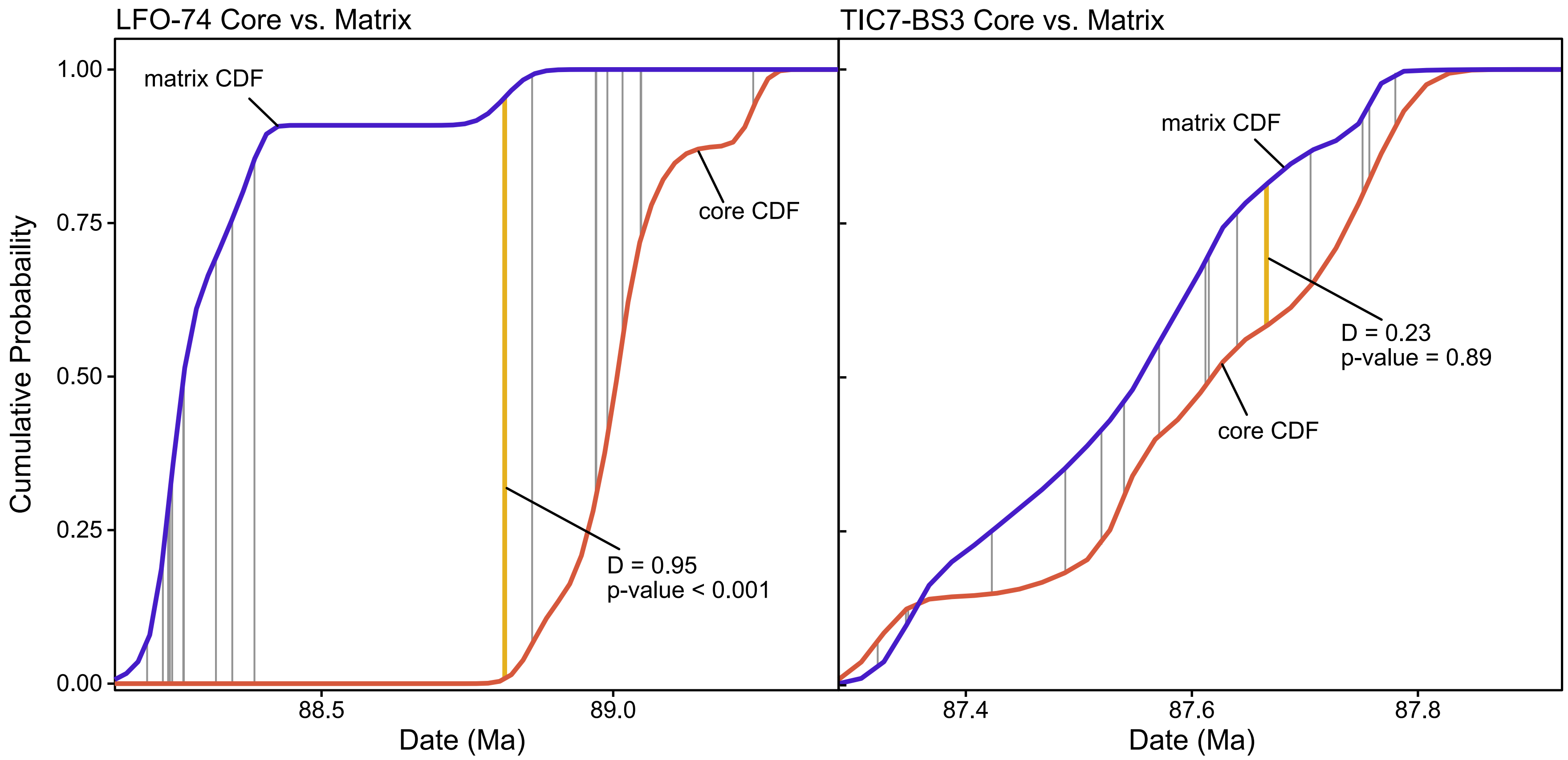

LFO-74 Core vs. Matrix
TIC7-BS3 Core vs. Matrix
Cumulative Probability
1.00
0.75
0.50
0.25
0.00
matrix CDF
core CDF
D = 0.95
p-value < 0.001
88.5
89.0
Date (Ma)
matrix CDF
D = 0.23
p-value = 0.89
core CDF
87.4
87.6
87.8
Date (Ma)

Figure6.

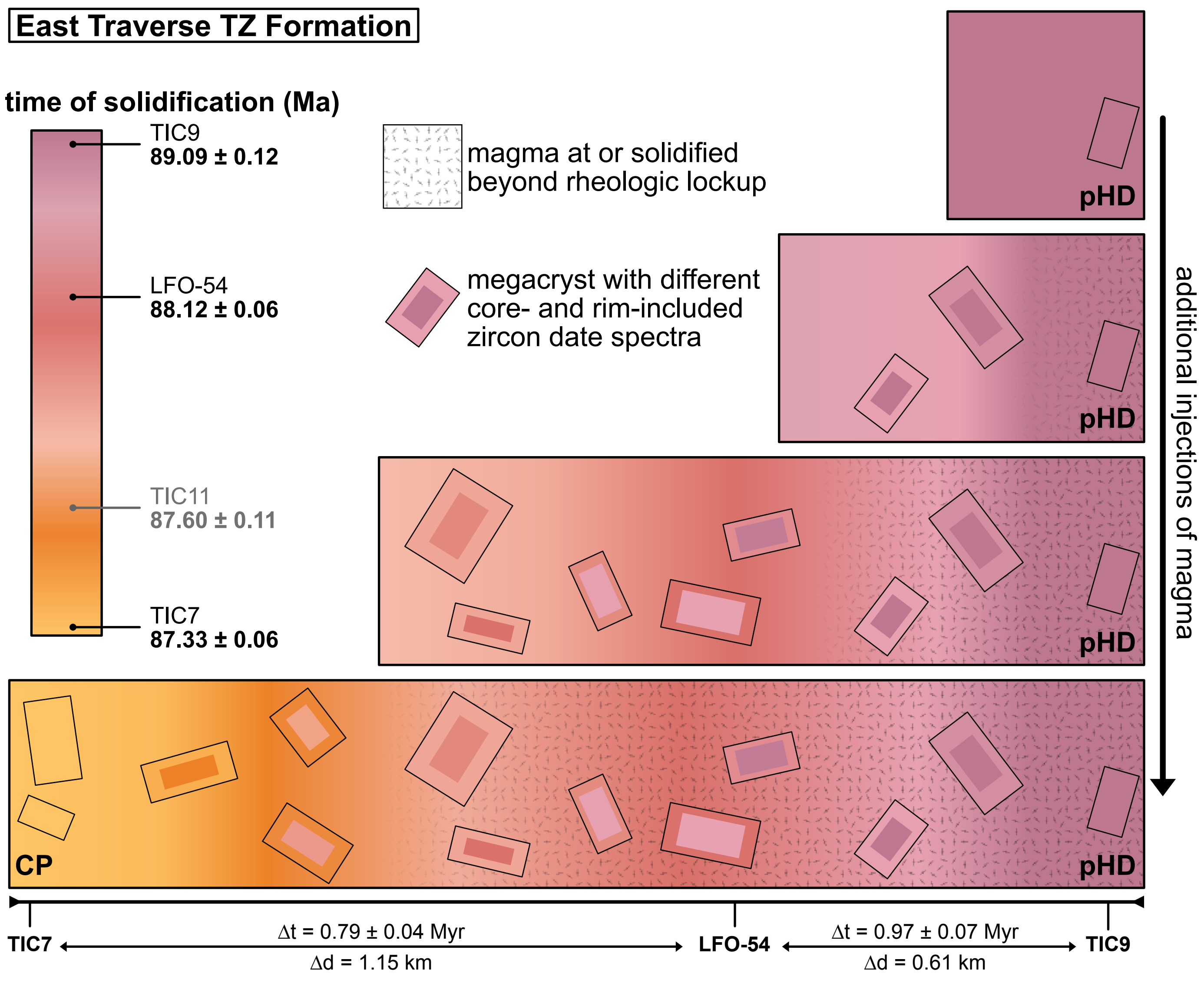
East Traverse TZ Formation
time of solidification (Ma)
TIC9
89.09 ± 0.12
LFO-54
88.12 ± 0.06
TIC11
87.60 ± 0.11
TIC7
87.33 ± 0.06
magma at or solidified beyond rheologic lockup
megacryst with different core- and rim-included zircon date spectra
pHD
pHD
pHD
CP
pHD
additional injections of magma
TIC7
Δt = 0.79 ± 0.04 Myr
Δd = 1.15 km
LFO-54
Δt = 0.97 ± 0.07 Myr
Δd = 0.61 km
TIC9